Coherent coupling of molecular spins with microwave photons in planar superconducting resonators

C. Bonizzoni[a,b], A. Ghirri[b] and M. Affronte[a,b]

[a]Dipartimento di Scienze Fisiche, Informatiche e Matematiche, Università di Modena e Reggio Emilia, via G. Campi 213/A, 41125, Modena, Italy;
[b]Istituto Nanoscienze-CNR, Centro S3, via G. Campi 213/A, 41125, Modena, Italy

ARTICLE HISTORY
Compiled January 10, 2018

ABSTRACT
Within the quest for solid state quantum systems to be used for fundamental as well applied research, molecular spins have recently emerged as a versatile platform with interesting performances in terms of quantum coherence and correlation. Molecular units provides well defined environment to electron spins and they represent elementary bricks for complex nano-architectures and nano-devices. Here we review our recent efforts and results on their efficient integration in circuits quantum electrodynamics and, more specifically, in reaching their coherent coupling with microwave photons in planar resonators. To monitor molecular spin performances over a wide temperature and magnetic field range we have first developed microwave planar resonators made of high T_c superconductors, obtaining excellent performances up to liquid Nitrogen temperature and magnetic fields up to 7 Tesla. Ensembles of several different molecular spins systems are then systematically tested. The regime of high spin-photon cooperativity is achieved with molecular spins diluted in non magnetic matrix at 0.5 K, while the strong coupling regime is observed with concentrated samples of organic radicals up to 50 K. The possibility to create coherent states among distinct spin ensembles is further explored in similar spectroscopic experiments. These results show that molecular spins can be efficiently integrated in quantum devices.

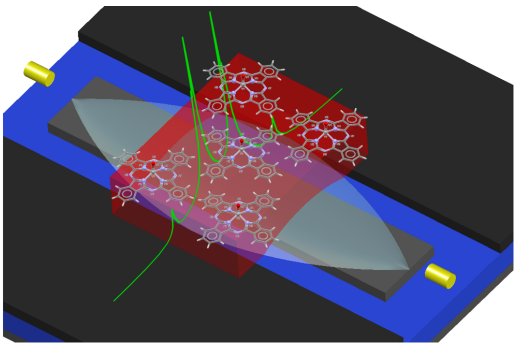

KEYWORDS
Molecular Spins, Coherent Spin-Photon Coupling, Circuit Quantum Electrodynamics, Electron Spin Resonance

CONTACT M. A. Email: marco.affronte@unimore.it

1. Introduction

The problem of coupling electromagnetic radiation with a two level system (TLS) is a central issue in Physics that can be schematized as the problem of two coupled harmonic oscillators. Interesting phenomena occur when the two systems are brought to resonance and, under specific conditions, genuine quantum phenomena emerge. Here we focus on coherent dynamics occurring when the coupling strength between the two systems (photons and TLS) is stronger than the damping of each of the two oscillators. This issue is now getting pivotal in quantum technologies since it determines the efficiency of the exchange of quantum information between photons and TLS. This problem has been largely explored in 3D cavities containing both photons and TLS. Renewed interest is now fed by circuit Quantum Electrodynamics (circuit-QED) technologies which, on one hand, allow the trapping of photons inside planar resonators and, on the other hand, the fabrication of TLS with different solid state platforms. This actually opens the way for the implementation of complex quantum architectures on a single chip. Along this way, although superconducting qubits are reliable mesoscopic TLS devices that efficiently couple to microwave (MW) photons in scalable architectures, an unprecedented step ahead in the miniaturization process would require the development of TLS at the molecular or the atomic scale. Here, spin centers constitute a reference test bed in the field. Color centers defects in inorganic matrices, eg. NV-center in diamond, Si or SiC, have been intensively studied in the last decades and showed great potentialities for applications both as hardware for quantum computing [1–3] and sensing [4, 5]. Key circuit-QED experiments have been recently performed with these systems [6, 7]. Molecular spins have attracted the interest of different communities in the last decades for the possibility to tailor their magnetic and quantum properties at synthetic level. In fact, they can be deposited and positioned on different substrates, and the bottom-up massive production of identical molecular units is relatively cheap. In the last decade, key experiments have shown that the spin coherent lifetime and entanglement can be tailored by suitable molecular engineering thus showing potentials for quantum technologies.
Here we present our early attempts to embed molecular spins in circuits QED. The article is organized as follows: in Section 2, specific molecular spin systems of interest for our experiments are presented and their spin dynamics are characterized. The development of high quality factor planar resonators with high-T_c YBCO superconductors and their characterization is presented in Section 3. In Section 4 we review key models frequently used to interpret spin-photons coherent dynamics. This can be useful for non experts and to fix key formulas used in the data analysis. The results of circuit-QED experiments performed with different ensembles of molecular spins are presented in Section 5. Finally, we conclude with a brief discussion (Section 6) and with a perspectives of this emerging field (Section 7).

2. Molecular spins for Quantum Technologies

Spins are prototypical quantum systems whose dynamics are fully described by quantomechanical operators, while the microwave technologies to address and manipulate them are widely developed and commercialized for applications in telecommunications and diagnostics. Thanks to the flexibility of synthetic chemistry, *molecular* spins offer the possibility to engineer the spin environment almost at wish and to design molecular

shells which, in turns, allows the positioning of spins on different platforms as required for hybrid devices.

2.1. Coherent spin dynamics in molecular systems

Although the characterization of the spin dynamics is known since long time thanks to the magnetic resonance techniques, the interest on controlling the coherent spin dynamics in molecular spin systems has attracted the interest of physicists only recently. Spectroscopic studies in both continuous wave (CW) and pulsed MW Electron Spin Resonance (ESR) experiments have been performed on specific classes of molecular systems aiming at finding molecular units with sufficiently long coherence life time for the spin manipulation. As discussed in textbooks, the dynamics of an isolated spin in a static magnetic field B_0 and under the stimuli of a probing electromagnetic radiation can be described by the Bloch equations, while the selection rules are provided by the conservation of the energy ($h\nu = g\mu_B \Delta S B_0$) and of the angular momentum. Just to fix some numbers: one electron spin ($S = 1/2$) in magnetic field B_0 of few hundreds of mT resonates in the GHz range of frequency. The resulting damped dynamics can be characterized by the transverse (T_2) and the longitudinal (T_1) life time, which account for the dephasing (spin-spin) and the relaxation (spin-phonon) mechanisms respectively (*vide infra*). Both contribute to the line broadening in CW-ESR spectroscopic measurements while, in real experimental conditions, sample and field inhomogeneities may also contribute to the broadening of the ESR lines.

2.2. Radicals

Radicals are open-shell molecules largely used as spin labels for biological systems. Typically, one unpaired electron (spin 1/2) is delocalized within an organic molecule making it very reactive. Yet, notable examples can be synthesized and they are sufficiently stable to be handled as bulk samples or dispersed in solution. Among these, di(phenyl)-(2,4,6-trinitrophenyl)iminoazanium (DPPH) is commercially available and actually used as standard in ESR spectroscopy. Nitroxides like the TEMPO family [8] or Nitronyl Nitroxides [9] are widely used in organic chemistry. More recently, (3,5-dichloro-4-pyridyl)bis(2,4,6-trichlorophenyl)methyl (PyBTM) radicals has also attracted much interest for its flexibility and multi-functionality [10].

2.3. Single-ion spin centers in molecular matrix

A further interesting class of molecular spin systems is constituted by metal centers in organic matrix. One of the most popular is the family of Metallophthalocyanines, MPc, that naturally exist in biological systems and are used for many applications. The spectroscopic performances of a series of MPc has been recently reported in [11]. Among this series, CuPc (Cu^{+2}, $S = 1/2$) has shown long coherence time at finite temperature also using a simple thick film preparation protocol [12]. Extremely long relaxation times were recently reported for VOPc derivative in which the VO double bond provides a spin 1/2 to the molecule [13]. The long T_1 and T_2 measured at room temperature allow to observe Rabi oscillations by pulsed MW experiments [13, 14]. A special class of molecules closely related to MPc is constituted by Lanthanide spin centers sandwiched between two Phthalocyanine planes, from which the nickname of double-deckers. In these molecules, the coordination of the trivalent Lanthanides (Ln)

provides well defined magnetic ground state given by combination of orbital and spin angular momentum which may result in a high magnetic moment for the metal center and large magnetic anisotropy. In general, pure ESR transitions are not allowed for Ln's due to the selection rules ($\Delta m_J = \pm 1$), and one remarkable exception (with other few Ln) is the case of Er.

2.4. Molecular Spin Clusters

It is worth to mention that the list of molecular spins with interesting performances, i.e. suitable for fast and coherent manipulation and qubit encoding, is increasing each year [15]. We just mention that also molecular spin clusters (i.e. molecules with a polynuclear core of metal centers behaving as a single spin) such as Cr_3 trimers [16] or heterometallic Cr_7Ni [17] (with spin 1/2 ground state), or Mn_{12} [18] and Fe_8 [19] (with a $S = 10$ ground state multiplet) also show multiple and spectroscopically distinguishable ESR transitions. This multi-level characteristic is an interesting feature which make spin clusters suitable platform also for multi-qubit (qudit) encoding. It should be also reminded that low-spin systems normally present a ground state split by hyperfine interaction and that multiple ESR transitions can be observed between mixed electron-nuclear spin states. Although this hardware is not fully scalable, it is however possible to pile one molecule on top of the other [20, 21] or to link two or more molecular units to create entangled spin states at supramolecular level [22, 23].

Finally it is worth to mention that molecular spins, being their properties sensible to a huge number of physical parameters, may also present multi-functionality. For instance the class of spin crossover systems [24] presents magnetic states that may switch with temperature, pressure, visible light and even magnetic field.

3. Superconducting circuits

3.1. Design and optimization of planar resonators

For spectroscopic measurements we use (simple metal) Ag/Alumina microstrip broadband transmission lines, that allow us to vary the probing frequency [25]. Superconducting resonators are widely used for circuit-QED experiments since they offer sharp resonant modes in the microwave frequency range [26]. They are obtained by cutting a superconducting line, delimiting a length equal to half of the desired wavelength of the fundamental mode. For our experiments we used high-T_c YBCO/Sapphire superconducting films whose fabrication is detailed in our previous work [27].
Commercial finite element electromagnetic simulation software (CST Microwave Studio) was used to design our planar resonators and was used to tune the resonant frequency in the desired range and to match the impedance with that of the external coaxial lines [28, 29]. The simulations are carried out with a full 3D 1:1 scale model of the resonators, in which the superconducting material is treated as a perfect electric conductor, while the substrate is modelled by taking the relative dielectric constant reported for Sapphire and assuming it constant in the 7-8 GHz range ($\epsilon_r = 9.4$ [30]). To partially account for dissipative effects, after preliminary simulation runs and experimental tests of the devices, the losses of the dielectric substrate are adjusted and fixed at $tan\ \delta = 10^{-5}$ in order to improve the agreement between the simulated and the measured values of the Insertion Loss and of the Q-factor.
The typical profile of the magnetic component of the simulated MW field for a copla-

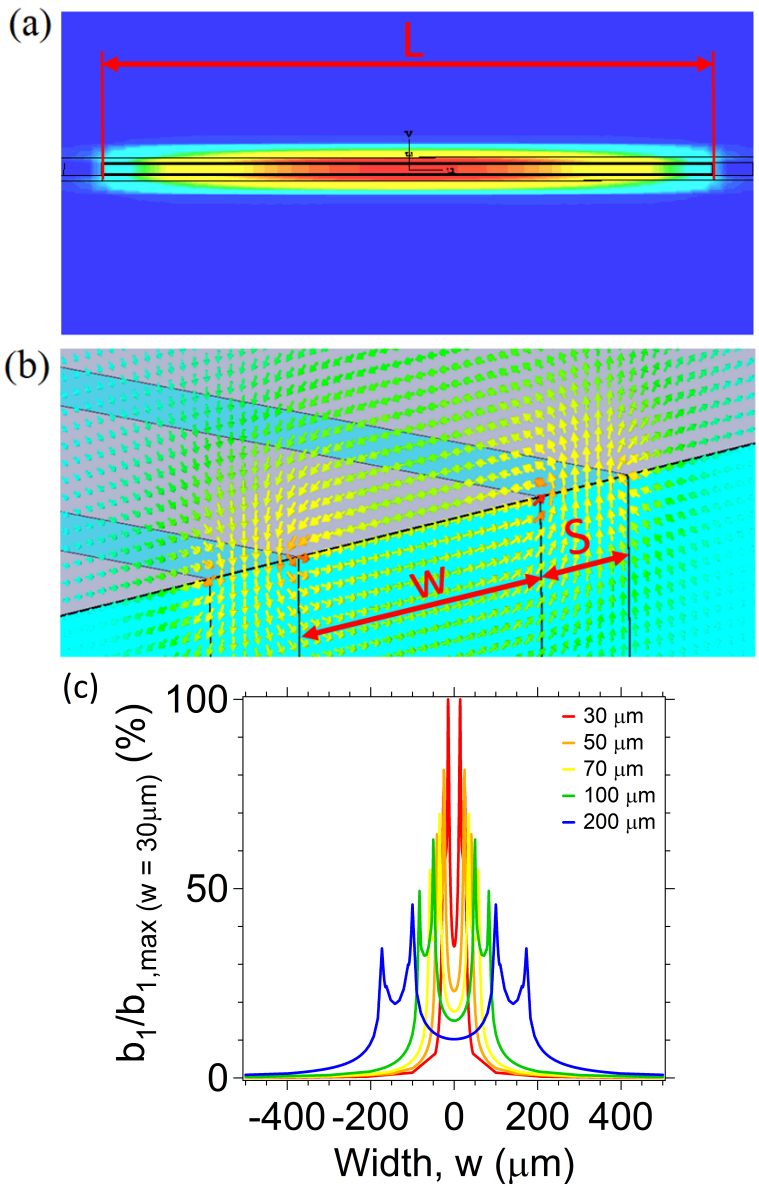

Figure 1. Simulation of the magnetic component of the MW field. The spatial distribution of the fundamental resonant mode in the plane of the superconducting film (a) and in a transverse section located in the middle of the resonator (b) are shown. The resonant strip is emphasized by the black rectangle. The color scale displays the normalized amplitude, with red corresponding to 100%. (c) Relative scaling of the simulated single photon magnetic fields ($b_1/b_{1,max(w=30\ \mu m}$) plotted along the transverse section of the coplanar resonator for different widths of the resonant strip. The fields are calculated at a distance of 5 μm from the surface and are normalized to the maximum of $w = 30\ \mu$m. Labels indicate the length (L), the width (w) and the gap (S) between the resonant strip and the ground planes of the resonator.

nar resonator is depicted in Fig. 1. The fundamental harmonic has maximum of the magnetic component at the center of the planar resonator whilst the maximum of the electric field component is achieved at the borders of resonator. The fundamental resonant mode can be approximated to quasi-Transverse Electromagnetic (TEM) mode, in which the electric field and the magnetic field components are lying in the plane perpendicular to the longitudinal axis of the resonator, with the magnetic field component wrapping around it. Simulations also allow us to estimate the relative scaling of the intensity of the field components at different heights from the surface and for different widths of the central YBCO strip (w) (Fig.1). It can be noticed that the MW are concentrated within few (hundreds of) microns (1-100 μm, depending on the size of the resonator) above the surface. By reducing w and the lateral gap (s), the MW magnetic field is concentrated in the center of the resonator as shown in Fig.1. In this way it is possible to increase the strength of the magnetic field component in a small volume.

3.2. Basic characterization and performances of YBCO resonator vs temperature and in magnetic field.

To characterize our resonator we use a commercial (Quantum Design, PPMS) cryomagnetic system with a custom made sample holder working at variable temperature (2-300 K) and static magnetic field (B_0) that, in this experimental configuration, lays parallel to the strip of the resonator (Fig. 2). For measurements below 1 K, we use a ^{3}He cryostat (Heliox VL by Oxford Instruments) in a vector (9+1+1)T magnet (Fig. 2) that allows us to orient the static magnetic field B_0 also perpendicular to the plane of the resonator. The resonator is packed into a copper shielding box, where the signal is injected and collected through two floating antennas [27, 32] (Fig. 2.a). The scattering parameters S_{11} (reflection) and S_{21} (transmission) are measured by a Vector Network Analyzer (Agilent Technologies 26 GHz VNA) with the microwave coaxial lines of the set-up (Fig. 2.b,c).
Hereafter, we will indicate with P_{in} the MW power reaching the input antenna, which is estimated by subtracting the attenuation of the input line from the output level of the VNA. The mean photon number, n, stored inside the resonant mode is calculated with the procedure reported in [27, 33]. To fix some numbers, $P_{in} = -13$ dBm corresponds to $n \approx 10^{10} : 10^{11}$ photons stored into the resonator.
In a preliminary study we have fabricated and characterized a series of coplanar resonators with different width w in order to optimize their characteristics for coupling with spin ensembles of different size. The experiments are carried out at 2 K. In principle, for an empty resonator, the parameters of the fundamental resonant peak can be obtained by fitting the frequency dependence of the transmission with Eq. 1 [34]. Since a completely different model (Eq. 2, see below) is used for the analysis of data of the resonators coupled to spin ensembles, we first check the reliability of the parameters obtained for the fits of our empty resonators within the two models (Fig. 3). Although clear deviations of the lineshape are visible in the tails of the signal ($T(\nu) \leq 35$ %) for Eq. 1, the peaks the values of the Q-factors (as FWHM), of the transmission and of the frequency are consistent within the two models. Fig. 3 shows the values of the resonance frequency (ν_0), quality factor (Q) and insertion loss [$IL = -S_{21}(\nu_0)$] obtained

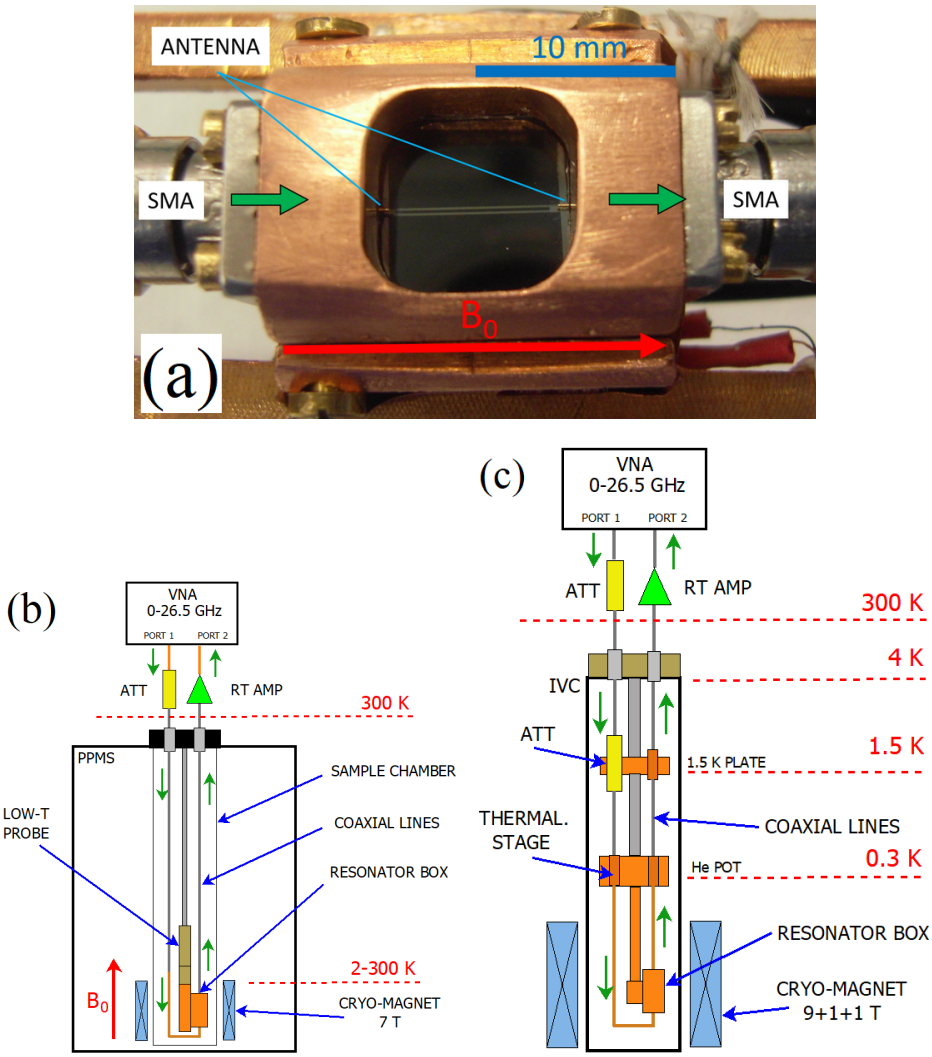

Figure 2. Experimental set-up used for circuit-QED experiments with spin ensembles. (a) Photograph of the shielding box with a coplanar resonator embedded inside. The MW signal (green arrows) is transmitted to the coplanar resonator by means of SMA connectors ended with two launching (floating) antennas. The position of the antennas can be adjusted to tune the coupling between the resonator and the feed lines. The red arrow represents the direction of the external static magnetic field. (b) Sketch of the QD PPMS set-up. The microwave is generated and analyzed by means of a the Vector Network Analyzer (VNA) connected to the low temperature coaxial line (green arrows) with attenuators (ATT) and amplifiers (AMP) installed at room temperature. from [27, 31]. (c) Sketch of the inner part of the Oxford Heliox VL cryostat, showing for clarity only the Inner Vacuum Chamber (IVC). The coaxial line is thermalized at the different temperature stages of the cryostat to reach 300 mK in correspondence to the resonator box. from [32].

as a function of w.

$$T(\nu) = -IL - 20\log_{10}\left[1 + Q^2\left(\frac{\nu}{\nu_0} - \frac{\nu_0}{\nu}\right)^2\right]. \quad (1)$$

The dependence of the quality factor as a function of w (Fig. 3.c) shows two different trends probably due to different effects. For the largest resonator ($w > 70$ μm) the decrease of the quality factor for increasing w can be likely related to the the increase of the radiation losses [33]. Conversely, for the resonator with $w < 70$ μm, the reduction of the quality factor with decreasing w can be possibly ascribed to the effect of irregular profiles in the lithographed YBCO structures introduced by the presence of grain boundaries [35–37].

The peculiarity of YBCO is to have a high critical temperature ($\simeq$ 90 K) and to be resilient to the application of an external magnetic field. To test these features, we measured the transmission spectra of a bare YBCO resonators with $w = 200$ μm and $s = 73$ μm in a temperature range between 2 and 70 K and in applied magnetic field up to 7 T [27]. The fit with Eq. 1 of the transmission spectrum at T=2 K and in zero field gives $\nu_0 = 7.75$ GHz, $Q = 20000$ and $IL = 16.5$ dB with $P_{in} = -13$ dBm. At low temperature these parameters slightly change under applied magnetic field as high as 7 T [Q(2 K,7 T)$\approx$ 18000], while the quality factor at 50 K in zero magnetic field is still above 10000 [27]. Preliminary measurements with a vector magnet shows that the quality factor is remarkably stable even when the magnetic field is applied out of the YBCO film plane (Fig. 4.d).

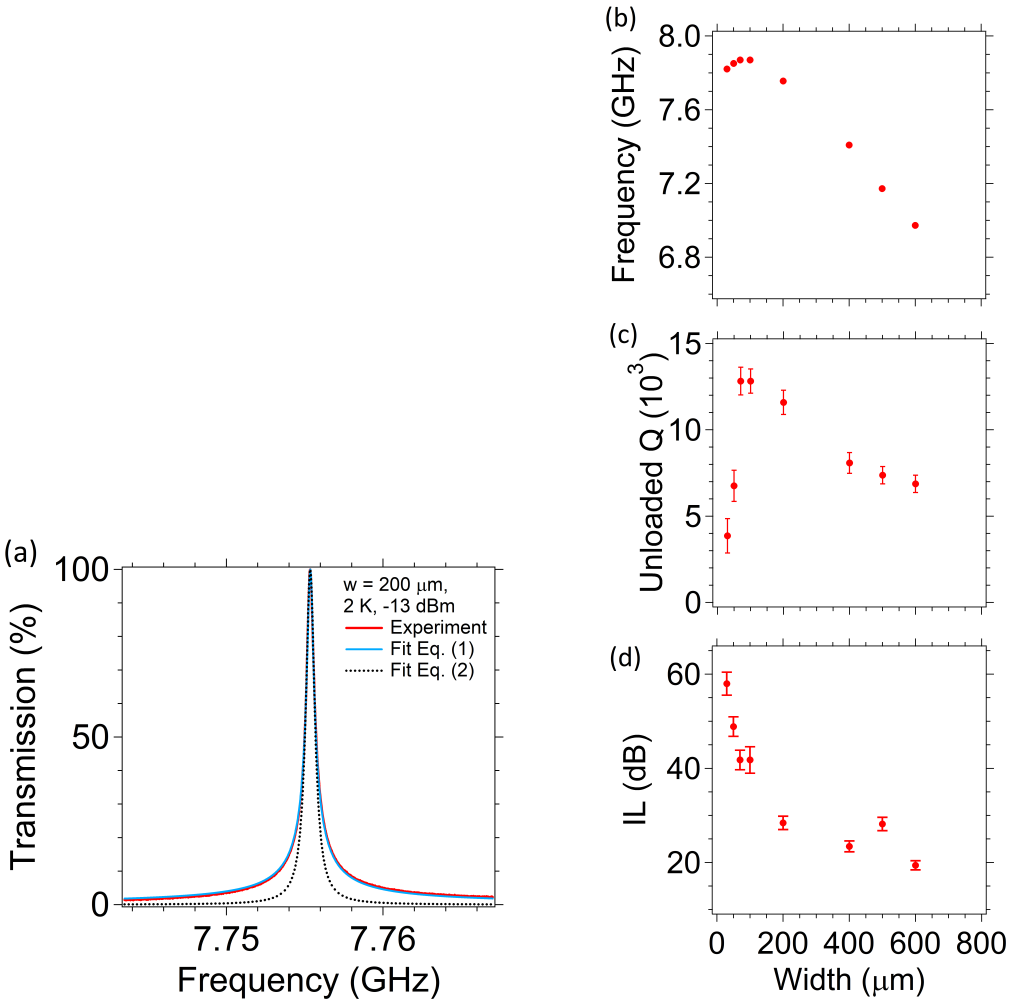

Figure 3. (a) Comparison between the fits of the transmission spectra obtained with Eq. 1 and 2 (black dashed line and blue line respectively) for a resonator with $w = 200$ μm at 2 K, -13 dBm and in zero magnetic field. (b,c,d) Dependence of the key parameters of YBCO coplanar resonators with respect to the width of the resonant strip. The values of resonant frequency (a), unloaded quality factor (b) and insertion loss (c) are extracted from transmission spectra taken at 2 K. The input powers used are $P_{in} = -13$ dBm ($n \approx 10^9 - 10^{11}$ photons) for $w \geq 70$ μm and $P_{in} = -43$ dBm ($n \approx 10^7 - 10^8$ photons) for $w \leq 70$ μm. Error bars in (b) are within the experimental points. Error bars in (c) are estimated according to the consistency of the values given by the fits performed with Eq. 1 or 2 and over different measurements, in a way similar to what previously done in [32]. Error bars in (d) have been estimated from the reproducibility of the transmission over different thermal cycles and antenna positions.

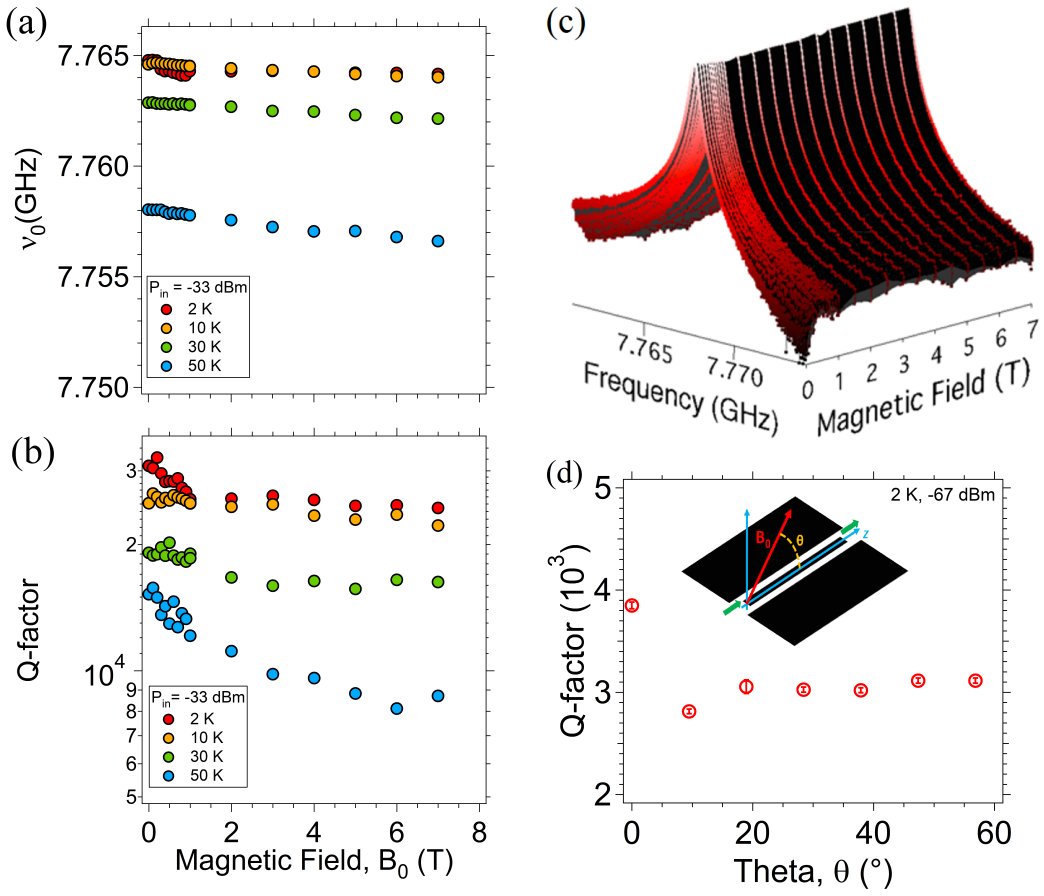

Figure 4. Plot of the resonant frequency (a) and quality factor (b) as a function of the static magnetic field for different temperatures. Data are taken on a YBCO/sapphire resonator with $w = 200$ μm, $s = 73$ μm, $L = 8$ mm. The results in (a) and (b) have been previously reported in [27]. (c) 3D plot of the resonant peak measured at 2 K as a function of the applied magnetic field for the same resonator of (a) and (b). (d) Dependence of the quality factor measured at 2 K and $P_{in} = -65$ for a YBCO coplanar resonator having $w = 600$ μm, $s = 800$ μm and $L = 8$ mm. θ indicates the polar angle between the static magnetic field and the resonator strip (see inset).

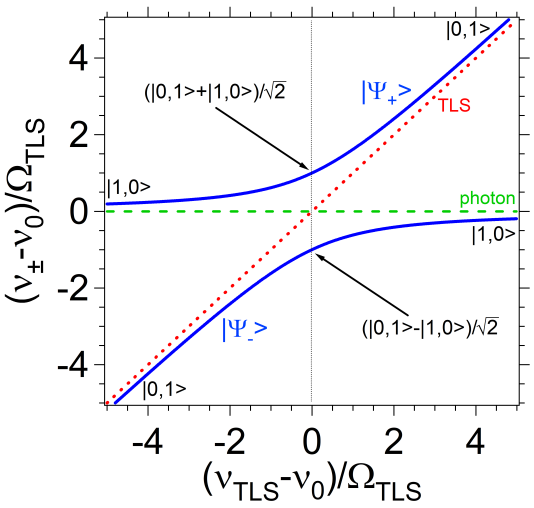

Figure 5. Plot of the eigenvalues of the Jaynes-Cummings Hamiltonian calculated as a function of the detuning for the simplest case of a TLS coupled to a single cavity photon. The observation of an avoided crossing on resonance follows from the presence of mixed spin-photon states.

4. Modelling

4.1. Semi-classical problem and Rabi oscillations

The general problem of coupling spins with electromagnetic radiation can be tackled by considering two coupled oscillators representing spins and photons embedded in a microwave resonator [38]. In a semiclassical approach, the quantum properties of the up and down orientations of a spin 1/2 can be represented by the $|\uparrow>$ and $|\downarrow>$ eigenstates of the S_z operator. Such a problem was first treated by Rabi [39]. The application of a static field B_0, let say along the z-direction, splits the energy levels of the two states according to the Zeeman effect. At sufficiently low temperatures, the lowest laying state is the mostly populated and the spin precesses around B_0 at the Larmor frequency $\nu_0 = g\mu_B \Delta S B_0/h$. A monochromatic radiation oscillating at frequency ν, when its magnetic field component B_1 is oriented in the xy plane, couples to the spin through its magnetic dipolar moment $\mu = g\mu_B \Delta S B_1$. The B_1 field induces magnetic dipole transitions between the $|\uparrow>$ and the $|\downarrow>$ states, making the spin oscillating up and down at the Rabi frequency $\Omega_R = g\mu_B B_1/\hbar$. The probability $P(t)$ to find the spin in its eigenstates oscillates as:

$$P(t) = \frac{\Omega_R^2}{\Delta_c^2 + \Omega_R^2} sin^2 \left(\sqrt{\Delta_c^2 + \Omega_R^2} \quad t/2 \right),$$

where $\Delta_c = 2\pi(\nu - \nu_0)$ is the detuning between the probing MW radiation and the Larmor frequency imposed by B_0. Note that at resonance ($\Delta_c = 0$) the Rabi frequency is entirely determined by B_1.

4.2. Hamiltonian for the spin-photon coupling

Since spins and photons are true quantum systems and we are interested in describing genuine quantum phenomena, such as the coherent coupling, we may represent photons

through the bosonic creation ($a^\dagger$) and annihilation (a) operators. This representation better describes the situation in which we have a finite number n of photons in a resonant cavity coupled to a generic Two Levels System (TLS), *e.g.*, in the case of our interest, a spin 1/2 . The general problem was originally treated by Jaynes and Cummings [40] who proposed to write the Hamiltonian of the simplest TLS-photon system as:

$$H = H_{ph} + H_{TLS} + H_{TLS-ph}$$

where:

$$H_{ph} = h\nu_0 a^\dagger a$$

,

$$H_{TLS} = h\nu_{TLS}\ \sigma^+_{TLS}\sigma^-_{TLS}$$

while the dipolar coupling between spin and photon can be written as:

$$H_{TLS-ph} = h\ \Omega_{TLS}\left(a^\dagger\sigma^-_{TLS} + a\sigma^+_{TLS}\right)$$

being Ω_{TLS} the TLS-photon coupling rate and $\sigma^{+,-}_{TLS}$ the rising $(+)$ and the lowering $(-)$ operators for the TLS respectively. While atoms may coherently couple with the oscillating electric field component though their electric dipole, the interaction of the spins with the magnetic component of the electromagnetic radiation turns out to be very weak, and coherent spin-photons oscillations are hard to be achieved. It can be shown, however, that the coupling of photon with an ensemble of TLS can be enhanced by a factor $\sqrt{N}$ with respect to Ω_{TLS}, being N the number of TLS centers of the ensemble (under the assumption that the number of photons in cavity is $n \ll N$) [41]. This problem was treated by Tavis and Cummings in term of collective modes of the TLS ensemble interacting with a resonant photon, in which the effective coupling strength is $\Omega = \Omega_{TLS}\sqrt{N}$ [42, 43]. This problem can be solved by a suitable choice of transformations [41, 44] and the eigenvalues of the system can be expressed as a function of the detuning between the TLS and the photon energies. In the simplest case of a single photon coupled to a single TLS this leads to the energies:

$$\nu_\pm = \nu_0 + \frac{1}{2}(\nu_{TLS} - \nu_0) \pm \frac{1}{2}\sqrt{(\nu_{TLS} - \nu_0)^2 + 4\Omega^2_{TLS}}$$

This implies that at resonance two separate branches appear in the spectrum, providing a characteristic signature for the coherent coupling between TLS and photons (Fig. 5). The eigenstates of the system turns out to be expressed by superposition of mixed TLS-photon states ($|m_{TLS}, n>= |1,0>, |0,1>$) in the form:

$$|\Psi_\pm >= \frac{1}{\sqrt{2}}\left(\sqrt{1 \mp a}\ |1,0> \pm \sqrt{1 \pm a}\ |0,1>\right).$$

This well represents the hybrid character of the coherent TLS-photon states, in which the degree of mixing is controlled by

$$a = \frac{\nu_{TLS} - \nu_0}{\sqrt{(\nu_{TLS} - \nu_0)^2 + 4\Omega_{TLS}^2}},$$

which depends by the TLS-photon detuning and by the coupling rate.

4.3. Linewidth and lineshape

A salient ingredient of the problem that should not be neglected is the fact that photons in cavity have finite lifetime due to the intrinsic cavity losses or simply the signal outgoing. Coherent oscillations of spins are also affected by the environment, which induces decoherence processes. Both mechanisms -largely discussed in textbooks- have the net effect to provide a finite linewidth to each oscillator. By convention, the κ constant accounts for the cavity linewidth while the γ parameter represent the line broadening of the spin resonance. The photon decay rate κ is related to the quality factor Q of the cavity, and we may define two contributions, κ_{int} and κ_{ext}, accounting for the internal losses (related to the geometry and the material of the resonator) and the external losses of the resonator (i.e. the signal outgoing through the feed lines) respectively. Thus, we have $\kappa = \kappa_{int} + 2\kappa_{ext}$. In an ensemble of independent spins, the γ parameter is related, at first instance, to the spin-phonon relaxation time (T_1) and to the dephasing (spin-spin) time (T_2) of the spins through the relation [45]:

$$\gamma_{hom} = \frac{1}{2T_1} + \frac{1}{T_2}\sqrt{1 + \gamma_e^2 B_1^2 T_1 T_2}.$$

The γ_{hom} value corresponds to the homogeneous broadening limit [46]. In real experiments, however, other mechanisms can contribute to the line broadening. These include inhomogeneities due to sample quality and to inhomogeneities of either MW field or static magnetic field. Since, in practice, these mechanism may well dominate over the homogeneous broadening, generally we have $\gamma \geq \gamma_{hom}$. Note that γ, γ_{hom} corresponds to the Half Width at Half Maximum (HWHM) of the spectral density of the spin ensemble. The mechanism of the line broadening influences also the shape of the line. This is a controversial point in literature [47] and, as a matter of facts, either Gaussian or Lorentzian lineshapes are used in the case of inhomogeneous broadened magnetic resonance spectra.

4.4. Input-Output formalism

In a typical circuit-QED experiment, the MW photons are injected and detected in a two port measure, in which the spin-cavity system is embedded between two terminals (input and output). The problem of determining the reflection and the transmission spectra can be solved by using the Input-Output formalism [48, 49]. In particular, in the case of Lorentzian spin transition, the transmission scattering parameter S_{21} is:

$$S_{21}(\nu) = \frac{\kappa_{ext}}{i(\nu_0 - \nu) + \kappa_{ext} + \frac{\kappa_{int}}{2} + \frac{\Omega^2}{i(\nu_S - \nu) + \gamma}}, \tag{2}$$

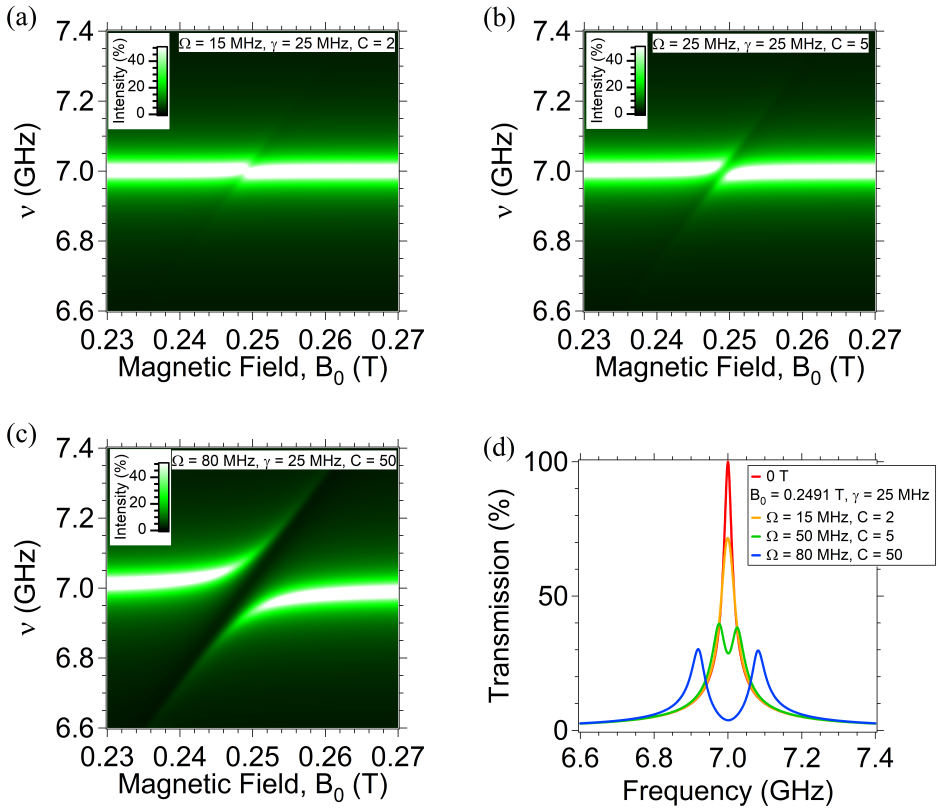

Figure 6. Evolution of the transmission spectral maps simulated under three different coupling regimes: weak coupling (a), high cooperativity (b) and strong coupling (c) regime. The spectral maps are calculated with Eq. 2 by fixing $\kappa_{ext} = 1 \cdot 10^7$ Hz, $\kappa_{int} = 1 \cdot 10^5$ Hz, $\nu_0 = 7$ GHz, $g = 2$, and $\gamma = 25$ MHz, while increasing values of the collective coupling strengths $\Omega = 15, 25$ and 50 MHz are used respectively for (a), (b) and (c). The comparison between the transmission spectra calculated at resonance is shown in (d).

where κ_{ext} and κ_{int} are the external and the internal decay rates defined above, γ is the HWHM spin linewidth (see above), Ω is the collective coupling rate between the spin ensemble and the photon and $\nu_S = g\mu_B B_0/h$ is the transition energy of the spin ensemble. This problem can be generalized in the case of more spins centers/ensembles and/or more photon modes inside in the cavity. The formalism and mathematical solutions have been also illustrated in recent works [50, 51]. Furthermore, the effect of the inhomogeneous broadening has been considered theoretically [52, 53] and possible cavity protection mechanism has been proposed [54].

4.5. Coupling regimes and cooperativity

We now have all the ingredients to understand results of spectroscopic experiments and to define different coupling regimes. The coherent coupling between spins and photons can be achieved if the strength of the spins-photon collective coupling rate, namely:

$$\Omega = \Omega_S \sqrt{N_{eff}}, \tag{3}$$

is larger than both the decay rate of the spin ensemble (γ) and of the photon in the cavity (κ). Since all these quantities have the dimension of frequency, the coherent coupling condition can be explicitly written as $\Omega > \kappa, \gamma$. It is also convenient to define the cooperativity as $C = \Omega^2/\kappa\gamma$, which allows us to distinguish between the different regimes at resonance. Note that, since in most of the experimental situations we have $\kappa < \gamma, \Omega$, the coupling regime effectively depends on the two latter parameters. When the coupling is weak, i.e. $\Omega \leq \gamma$, we have incoherent absorption and emission of photons by the spin system. This is the usual working condition in ESR experiments and the signal observed is a dispersive spectrum. Here we have $C \leq 1$. For stronger coupling strengths $\Omega \approx \gamma$ (or also $\Omega \geq \gamma$) the system enters in a high cooperative regime, in which $C > 1$. In this case, the spectrum presents a characteristic splitting in two branches, which evidences the presence of hybrid spin-photon states and coherent dynamics [42, 55]. When $\Omega \gg \gamma$ (and, hence $C \gg 1$) we enter in the so called strong coupling regime, and the splitting between the two branches gets more evident. The different spectroscopic features obtained under the different coupling regimes are show in Fig. 6.

5. Results

In the weak coupling regime, planar resonators and broadband transmission lines (see Section 3) can be used to characterize the spin transitions in bulk samples of molecular spin centers. We use either Ag/Alumina microstrips or YBCO/Sapphire coplanar resonators by means of the experimental set-ups shown in Fig. 2. Bulk samples, either crystals or bulk pellets, are glued on top of the central strip with a small amount of Silicon grease or Apiezon N grease.

5.1. Preliminary ESR-like spectroscopy on Cr_3 trimers

We first test the molecular trimer of $Cr_3OPIV_6(H_2O)_3PIV$, Cr_3 in short. In this molecule, three Cr^{3+} ($S = 3/2$) ions in triangular configuration are antiferromag-

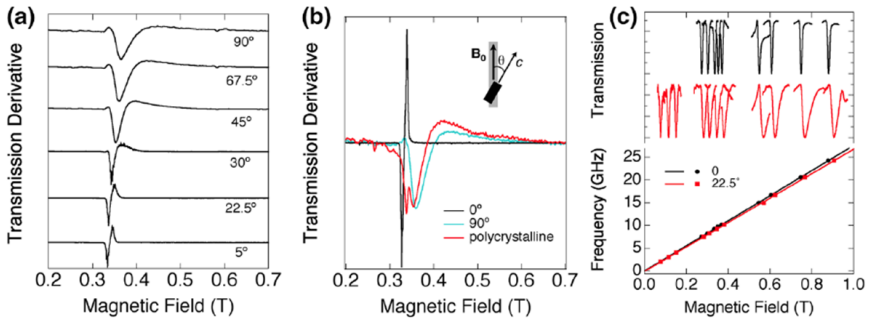

Figure 7. Magnetic resonance spectra of molecular Cr_3 samples. The experimental results have been obtained at 2 K with an Ag/Alumina microstrip resonator ($\nu_0 = 9.215$ GHz) and a Ag/Alumina broadband transmission line [25]. (a) Magnetic field dependence of the derivative of the transmission with respect to the magnetic field measured for different θ by means of a microstrip resonator. θ corresponds to the polar angle between the c-axis of the crystal and the static magnetic field [inset of (b)]. (b) Comparison between $\theta = 0°$ and $90°$ and the transmission spectra obtained with a polycrystalline sample of Cr_3. (c) Measured spectra (top) and resonance field (bottom) obtained for different probing frequencies and angles ($\theta = 0°$ and $22.5°$) by means of a broadband Ag/Alumina transmission line. Reproduced with permission from Ref. [25].

netically coupled each other giving rise to two doublets as lowest lying energy levels [16]. The absorption spectrum obtained with the Ag resonator ($\nu_0 = 9.215$ GHz) shows the characteristic line shape of a doublet transition centered at 0.33 T (Fig. 7), corresponding to $g_{\|} = h\nu/\mu_B B_{\|} = 1.97$, with a linewidth of 12 mT (equivalent to $\gamma = 167$ MHz). By aligning the c-axis of the crystal at different angles θ with respect to B_0 we can monitor the angular dependence of the absorption line: as θ increases, the transition shifts toward higher fields and gets broader (Fig. 7). Spectra at different frequencies were obtained by using a broadband Ag transmission line (Fig. 7). The signal in this case is much weaker than what obtained with a resonator, yet information obtained are quite complementary: a linear behavior, described by $\nu = g\mu_B B/h$, is clearly observable. For $\theta = 0$ we have $g = g_{\|} = 1.97$ (black line in Fig. 7), while for $\theta = 22.5°$ (red line) $g = \sqrt{g_{\|}^2 \sin^2\theta + g_{\perp}^2 \cos^2\theta} = 1.65$ (with $g_{\perp} = 1.6$). These results have been previously reported in [25].

5.2. Er^{3+} magnetic centers.

The effective number of spins (N_{eff}) involved in the experiments and their concentration in a bulk sample play a key role and they need to be finely tuned to obtain high cooperative regime: on one hand we need the spins to be sufficiently dispersed to minimize dipole-dipole interaction and consequent line broadening but, at the same time, the collective coupling $\Omega \propto \sqrt{N_{eff}}$ (Eq. 3) needs to be enhanced as well. Besides the $\sqrt{N_{eff}}$, the strength of the coupling with electromagnetic radiation is proportional to the intrinsic g-factor of a single magnetic center according to [56]:

$$\Omega_s = g\frac{\mu_B}{\sqrt{2}} \left| < E|\vec{b_1} \cdot \vec{J}|G > \right|. \tag{4}$$

Here $|E>, |G>$ are the excited and the ground magnetic states respectively, $\vec{b_1}$ is the single photon magnetic field generated by the resonator and $\vec{J}$ is the total angular

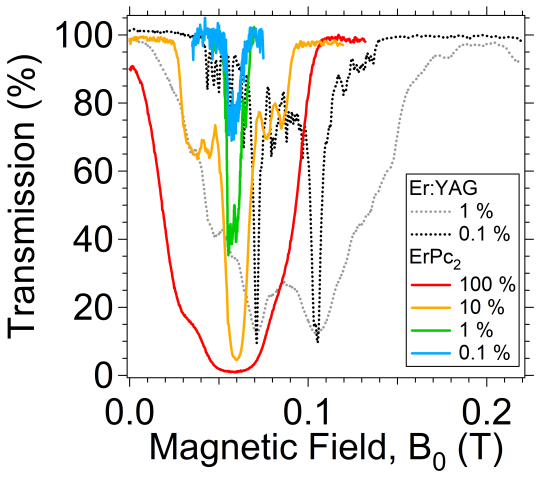

Figure 8. Comparison between the transmission spectra obtained at 2 K for molecular $ErPc_2$ crystals (100 %, 10 %, 1 % and 0.1 % concentrations) and for Er:YAG inorganic crystals (1 % and 0.1 % doping percentage). For the $ErPc_2$ sample the c-axis of the crystal is parallel to the magnetic field $\mathbf{B_0}$, while for the Er:YAG crystals the $< 111 >$ axis parallel to $\mathbf{B_0}$. Part of the $ErPc_2$ spectra have been previously reported in [31].

momentum of the molecule. This implies that, in principle, the coupling can be enhanced by a suitable choice of the magnetic center, by taking those with the largest g-factor, i.e. Lanthanides.

To explore this possibility, we investigated the coupling between YBCO superconducting resonators and crystals of molecular $ErPc_2$ double-deckers diluted in a diamagnetic YPc_2 matrix with different concentrations (100 %, 10 %, 1 % and 0.1 %). In the $ErPc_2$ molecules, Er^{3+} ions have a ground J=15/2 multiplet with a set of non degenerates Kramers doublets, where the fundamental one is well separated (30 K) by the first excited one, and acts as an effective 1/2 spin. This ground doublet has an easy plane anisotropy with large effective Landé g-factor component (≈ 9.5).

Fig. 8 shows different transmission spectra obtained on $ErPc_2$ crystals with different concentrations. The resonant peaks are centered at 0.06 T, corresponding to a g-factor component of 9.59 (close to the easy plane). For the concentrated sample (100 %), the broad linewidth (0.08 T) is due to the strong influence of dipole-dipole interaction among the spins. As the magnetic centers get more diluted, the linewidths gets sharper: for the 0.1 % concentration the width is significantly reduced down to 0.01 T, although the signal gets smaller because of the lower number of spins. The shape of the signal is different with respect to the highest concentrations (i.e. 100 % and 10 %), since 3 main lines, due to hyperfine coupling with Er^{3+} nuclear spin, can now be resolved.A detailed discussion of the $ErPc_2$ results have been previously reported in [31].

It's interesting to compare these spectra with the ones obtained in similar experiments performed on a Yttrium-Aluminum-Garnet (YAG) crystal doped with Er^{3+} impurities (hereafter, Er:YAG). The crystal environment in this case is purely inorganic, yet the ground state of Er^{3+} is still an effective $m_{J=1/2}$ doublet with lower Landé g-factors with respect to $ErPc_2$. We used two crystals with doping percentages of 1 % and 0.1 %, respectively. The YAG crystal structure comprises 6 inequivalent Er^{3+} centers, giving a ESR spectrum with 6 main resonances and additional hyperfine splitting [57–59]. The simplest situation is obtained with a static magnetic field applied parallel to the $< 111 >$ direction (Fig. 8). For the 1 % Er:YAG specimen

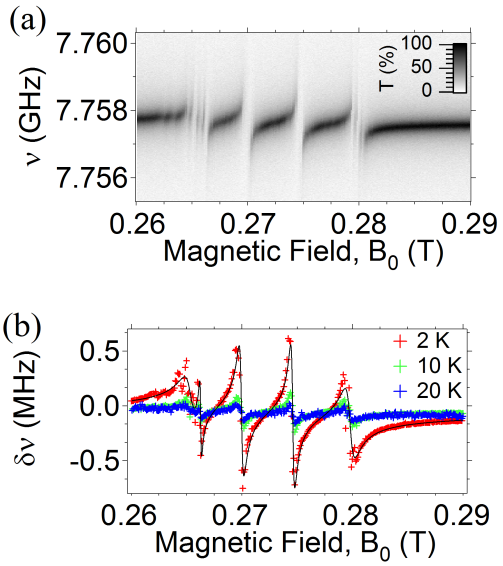

Figure 9. Transmission spectroscopy on crystals of $Cu(mnt)_2$ deuterated molecules diluted at 2% in a non-magnetic analog. (a) Transmission spectral map measured at 2 K by means of a YBCO coplanar resonator ($w = 200\mu$ m, 7.75 GHz) with microwave power $P_{in} = -63$ dBm. The four $|-m_S, m_I> \rightarrow |-m_S+1, m_I>$ transitions are visible, while additional lines at $B_0 \approx 0.265$ T and $B_0 \approx 0.28$ T are due to the presence of two inequivalent sets of molecules within the crystal structure. (b) Plot of the frequency shift $\delta\nu = \nu - \nu_0$ as a function of the static magnetic field for different temperatures. Solid line is a fit with the model described in Ref. [31]. Figure reproduced with permission from Ref. [31].

the spectrum presents two broad peaks centered at 0.07 T and 0.12 T, respectively. A further decrease of the dilution to the 0.1% refines this spectrum, resulting in two narrow transitions (again, along the $< 111 >$ direction) and additional multiple hyperfine signals given by the $I \neq 0$ nuclear spin isotopes (^{167}Er, I = 7/2 and n.a. = 23 %). We note that the width of these resonance is comparable to the equivalent 0.1% $ErPc_2$ samples. Although this comparison is not conclusive, we learn that the use of organic environment is not detrimental for magnetic centers.

5.3. Hyperfine splitting in $Cu(mnt)_2$ spectra

The previous discussion evidences some role of hyperfine coupling between electron and nuclear spins. Interestingly, coordination chemistry may provide tools to control nuclear spins in the ligands and in the metal center by suitable isotope substitution. For instance, one possible choice is to avoid nuclear spins in the ligands, which are known to often introduce excessive splitting of the absorption lines and an uncontrolled line broadening [14, 60, 61]. Conversely, fine control of nuclear spin in the metal center may give rise to well defined split of the resonance lines that, in turns, can be exploited for multiple qubit encoding.

In the next experiment [31] we used the coordination compound $(PPh_{4-d20})_2[Cu(mnt)_2]$ (where mnt^{2+} = maleonitriledithiolate or 1,2-dicyanoethylene-1,2-dithiolate), containing Cu^{2+} ions. We used a crystal of $Cu(mnt)_2$ diluted into the diamagnetic analogue $(PPh_{4-d20})_2[Ni(mnt)_2]$ with a concentration of 2 % and with deuterated PPh_4^+ counter ions. The anisotropic hyperfine interaction between the electron ($S = 1/2$) and the nuclear spin ($I = 3/2$) of the Cu^{2+} ion gives rise to a quartet [62]. The transmission spectra of Fig. 9 shows four main structures between

0.24 T and 0.29 T, consistently with the expected $g = 2.04$ and hyperfine splitting of Cu^{2+}. Although the linewidth is relatively sharp ($\gamma = 6$ MHz), no evidence of coherent coupling was found at 2 K. Data analysis [31] allows to extract the collective coupling rate for the two main central transitions, giving $\Omega = 2.7$ MHz, which is only slightly smaller than γ.Further details about the transmission spectroscopy performed on $Cu(mnt)_2$ samples have been previously reported in [31].

5.4. Reaching High cooperativity with VOPc molecules

In a system of diluted spin centers, the spin-photon coupling strength effectively increases by lowering the temperature. In fact, the effective number of spins indeed depends on temperature according to the Brillouin law that, for a $S = 1/2$ paramagnetic system, reduces to:

$$N_{eff}(T) = N_0 p(T) = N_0 \tanh\left(\frac{h\nu}{2k_B T}\right), \tag{5}$$

this suggests how it is possible to increase the effective number of spins aligned with the static field [i.e. the spin polarization $p(T)$] for a fixed concentration of spin centers. In the next experiment, we have investigated more deeply the temperature dependence (from 30 K down to 0.5 K) of a Vanadyl Phthalocyanine (VOPc) that has recently shown long coherence time and Rabi oscillations even at room temperature in solid dispersion [13, 64]. Polycrystalline samples of VOPc diluted in its equivalent diamagnetic host (Titanium Phthalocyanine, TiOPc) were studied by using our YBCO resonators ($w = 200\ \mu$m$, \nu_0 \approx 7.7$ GHz and $Q \approx 10000$ and $w = 600\ \mu$m$, \nu_0 \approx 7$ GHz and $Q \approx 6000$ at 1.5 K) [32]. The transmission spectrum at 2 K shows a multi-folded pattern of resonances at $g \approx 2$, as expected from the powder spectrum of a spin $S = 1/2$ with additional hyperfine coupling to the $I = 7/2$ nuclear spin of the VO^{2+} group [13] (Fig. 10). The analysis of the central line reveals that the linewidth remains constant at $\gamma = 30 \pm 4$ MHz from 30 K down to 0.5 K, while the collective coupling rate progressively increases by lowering the temperature (according to Eq. 5). We reach $\Omega = 21 \pm 3$ MHz and a cooperativity $C \approx 15 > 1$ at 0.5 K, confirming that the high cooperativity regime is achieved at this temperature. This fact is corroborated by the direct observation and appearance of the two branches in the dispersion and of the Rabi splitting in the central line, as shown in Fig. 11.

This result is particularly significant if we compare it to what obtained with spin impurities in inorganic matrix (namely NV centers and Er^{3+} in inorganic crystals) in similar circuit QED experiments reported in literature [65–68]. In fact, the cooperativity values found at 0.5 K for VOPc are comparable to the ones reported for color centers in inorganic hosts, although the latter experiments are performed in the mK temperature range. We can safely extrapolate the collective coupling Ω to lower temperatures as shown in Fig. 10 (dashed lines) and find that strong coupling regime can be achieved for VOPc in the mK temperature range (Fig. 10).The full set of results and the discussion about VOPc samples have been published in [32].

5.5. DPPH and PyBTM organic radicals

Experiments described so far have been performed on bulk crystals ($ErPc_2$, $Cu(mnt)_2$) or powders (VOPc) specimens with $\approx$ few mm size. Additional investigations show

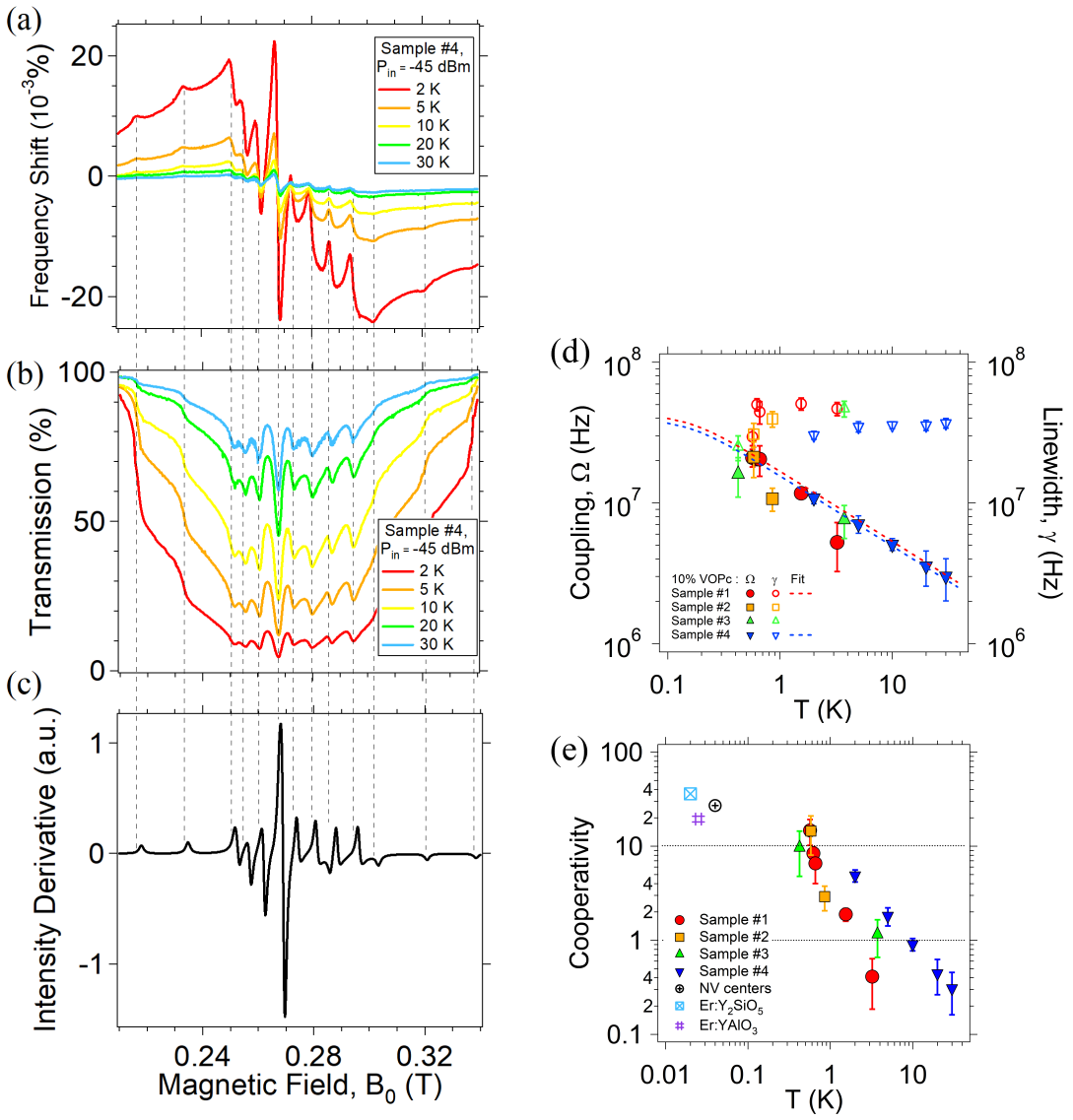

Figure 10. Transmission spectroscopy on 10% VOPc:TiOPc solid dispersions in the 0.5-30 K temperature range. Magnetic field dependence of frequency shift (b) and transmission (b) measured in the 2-30 K range by means of a YBCO coplanar resonator. The position of the observed resonances corresponds to that obtained from the Easy Spin simulated spectrum [63] shown in (c), which, in turn, is obtained with the g, A parameters of the Hamiltonian reported in [13]. (d) Plot of the collective coupling rate and spin linewidth as a function of the temperature for different samples of 10% VOPc:TiOPc solid dispersions (Samples from #1 to #4). Dashed lines show the temperature dependence of the coupling strength calculated from Eq. 3 and 5. (e) Cooperativity-vs-temperature plot derived from the values in (d). Reproduced under CC licence from Ref. [32].

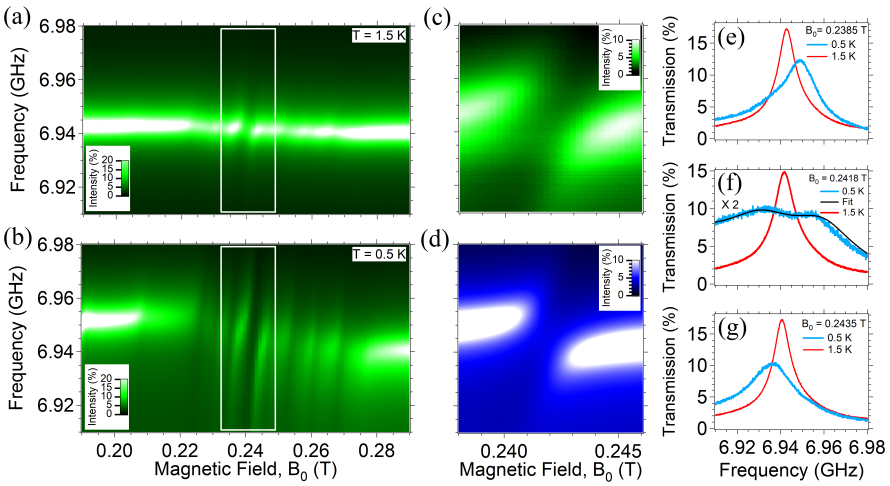

Figure 11. Transmission spectroscopy on 10% VOPc:TiOPc solid dispersion at 1.5 K (a) and at 0.5 K (b). The main line at 0.5 K is magnified in (c), which clearly shows two branches that indicate the reaching of the high cooperativity regime. The corresponding transmission spectrum shows a splitted peak (f). Curve fitting performed with Eq. 2 [(d) and black line of (f)] allows the extraction of the Ω and the γ parameters. Reproduced under CC licence from Ref. [32].

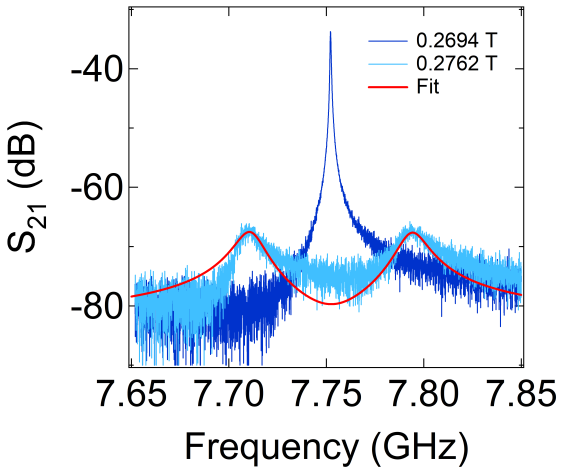

Figure 12. Transmission spectroscopy of a DPPH powder sample in the strong coupling regime. The Rabi splitting of the transmission spectrum is clearly visible at resonance (light blue) with respect to a spectra taken off resonance (dark blue). Data are measured at 2 K by means of a YBCO coplanar resonator ($\nu_0 = 7.75$ GHz, $Q \approx 30000$) with microwave power $P_{in} = -13$ dBm. Red line is a fit based on Eq. 2. Reproduced with permission from Ref. [27]

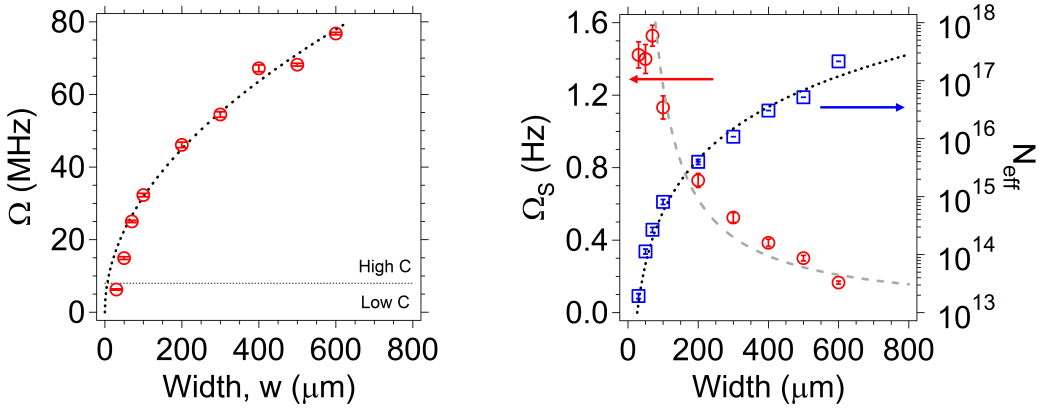

Figure 13. Scaling of the coupling parameters measured between YBCO coplanar resonators with different sizes and a pellet of concentrated DPPH powder at 2 K.(a) Dependence of the coupling rate, Ω, as a function of the width of the resonant strip. Dashed line is a guide for eyes based on a $\Omega \propto w^{1/2}$ law. (b) Single spin coupling rate, Ω_S, and effective number of spins, N_{eff} as a function of the width. Dashed lines are guides for eyes based on a $N_{eff} \propto w^3$ law (black one) and on a $\Omega_S \propto 1/w$ law (grey one).

that inhomogeneities of both the static [27, 32, 51] and the oscillating field occur at this length scale. Moreover, in powder samples molecules are randomly oriented and, although the single ion magnetic anisotropy can be relatively weak, this also contributes to line broadening. The presence of additional hyperfine split contributes to increase the broadening effects. It turns out that the linewidth in our spectroscopic experiments are not dominated by intrinsic coherence time of single molecule (T_1, T_2 and γ_{hom}) but rather by inhomogeneity effects. An effective way to bypass this problem is to exploit exchange narrowing effect [69–72] in concentrated molecular systems with intermolecular interactions. Intuitively, exchange coupling between neighbouring molecules induces collective spin excitations that are delocalized and less suffer the effects of the inhomogeneities. This results in an effective narrowing of the ESR resonance line, i.e. small γ values. This effect is well documented for concentrated organic radicals, which show typical ESR linewidth of less than 10 MHz at 2 K [73, 74]. For instance, this is the case of commercial di(phenyl)-(2,4,6-trinitrophenyl)iminoazanium (DPPH) that is widely used as marker in ESR spectroscopy.

In order to check this effect, we have performed circuit-QED experiments on DPPH organic radical powders using our standard 7.75 GHz YBCO resonator. The Rabi splitting of the transmission was observed between 2 and 50 K, and the amplitude of the splitting exceeds 80 MHz at 2 K (Fig. 12). The cooperativity value of $C \approx 500 \gg 1$ well demonstrates that the strong coupling regime is achieved.

To consolidate this result we have also performed a systematic investigation by changing the width of our YBCO coplanar resonator. The coupling rates obtained between a DPPH pellet (100 % concentration, diameter $\phi = 5\ mm$) and YBCO coplanar resonators with different widths are shown in Fig. 13. We observe that the collective coupling vanishes as the size of the resonator is shrank. This should not be surprising since the shrinking of the planar resonator implies a reduction of effective sample volume, i.e. of number of spins coupled to the resonator. Conversely, the intensity of electromagnetic radiation increases in proximity of the borders when the width of the resonator is shrank (Fig. 1). Electromagnetic simulations help us to estimate the effective number of spins involved and to find a tradeoff between these two competitive effects. For instance, with CST software the magnetic sample is

considered as a solid with relative dielectric constant $\epsilon_r = 1$, and the integral of the magnetic field distribution over the sample volume is calculated with the software's tools. The volume obtained is used, with the spin density of the sample, to estimate the number of spins N_0 involved into the magnetic coupling (see Eq. 5). Given the temperature dependence of the spin polarization, this data are used to estimate the effective number of spins coupled to the resonator for a given temperature (Fig. 13.b). Finally, according to Eq. 3 also the single spin coupling rate Ω_S is evaluated. The results (Fig. 13) allows us to better understand the decrease of the coupling rate. In fact, the single spin coupling effectively increases as the resonator is narrowed but, since the volume of the resonant mode is also reducing, the decrease of the number of spin is the dominant term.This is also corroborated by the scaling laws plotted in Fig 13 (dashed lines). For the single spin coupling rate the law $\Omega_S \propto |\overrightarrow{b_1}| \propto 1/w$ is obtained through Eq. 4 under the approximation of the resonant strip as a thin wire [75]. The scaling of the collective coupling rate as $\Omega \propto w^{1/2}$ comes from Eq. 3 and 4, assuming a dependence of the number of spins by the volume ($N_{eff} \propto w^3$). Circuit-QED experiments with DPPH radicals have been recently repeated by other groups [76] confirming that strong coupling regime can easily be obtained using this organic radical.
It is worth to mention that we were also able to observe strong coupling regime by using another organic radical (3,5-dichloro-4-pyridyl)bis(2,4,6-trichlorophenyl)methyl (PyBTM) for which we obtained $\gamma \approx 3$ to 8 MHz, $\Omega = 80$ MHz (at 2 K) and cooperativity value C up to 4300 (at 2 K, depending on the number of spin in the sample). Further details concerning these results have been reported in [51].

5.6. Coupling distant spin ensembles

Interestingly, DPPH and PyBTM organic radicals have very similar g-factors (2.0037 and 2.003 respectively) and the resolution of our experiments allows to experimentally resolve this small difference. This lead us to ask to ourselves what happens when two spin ensembles with slightly different spectroscopic feature are put in the same cavity. These experiments were performed with two spectroscopically or spatially distinguishable spin ensembles at 2 K on the same 7.75 GHz YBCO coplanar resonator used in the previous sections. Fig. 14 shows the different configurations used in each experiment. Firstly, the Rabi splitting with only two branches is obtained by placing two halves of a DPPH pellet at the center of the YBCO resonator. In this case the spectroscopic features are perfectly equivalent to the ones shown in Fig. 12, i.e. to the ones given by a unique spin ensemble. Yet, when one half of the DPPH pellet is replaced with one with PyBTM, we observe the appearance of an additional bright mode in the center of the two original branches. When two halves of the same PyBTM pellet are placed at extremes of the resonators we -again- observe the additional third mode between the two branches. These results can be interpreted with the help of a generalized version of the Tavis-Cummings Hamiltonian red, and lead to a generalized version of Eq. 2 in which two distinguishable (either spectroscopically or spatially) spin modes and one photon mode of the cavity are included [51]. The presence of multiple bright modes, along with the values of the entropy calculated for each spin and photon mode [51], confirms the coherent coupling between multiple spin ensembles through the cavity photons. These results and discussion concerning the remote coupling of molecular spin centers have been previously reported in [51].

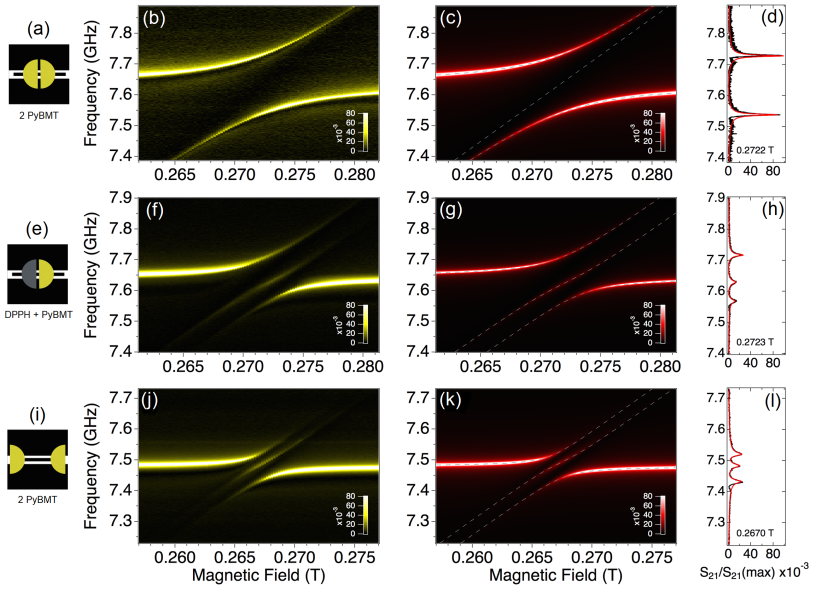

Figure 14. Transmission spectroscopy performed with multiple spin ensembles coupled to the standard 7.75 GHz YBCO resonator. (a,e,i) shows the positions and the ensembles used in the experiments. (b,f,j) Transmission spectral maps measured at 2 K for the different configurations of the spin ensembles. In the case of (f) and the (j) three branches are clearly visible, denoting coherent spin-photon mixing between the two spin ensembles and the resonator. (c,g,k) Spectral map simulations based on a generalized version of Eq. 2. (d,h,l) Transmission spectra measured at resonance for the three different configurations of the spin ensembles. Red line are fit based on the same generalized Eq. 2. Reprinted with permission from Ref. [51].

5.7. Strong Coupling with high order harmonics

In the next series of experiments we revisit the problem of Sec. 5.6 by using a single concentrated DPPH powder sample (100 % concentration, pellet with diameter $\phi = 5\ mm$) coupled to the three lowest harmonics of a YBCO microstrip resonator ($w = 700\mu$m and $L = 7$ mm, as in Fig. 15). The profile of B_1 along the longitudinal axis of the resonator indeed effectively addresses different, spatially separated, spin sub-ensembles. In this way, multiple mixed spin-photon modes are created and their number increases with the order of the harmonic. Interestingly, the use of high order harmonics may be relevant for applications in which multi-frequency quantum bus or multi-frequency qubit encoding are needed [77–79]. The spectroscopic results are shown in Fig. 15. Here, we can notice that the number of bright modes actually increases with the increasing order of the harmonic. We can fit these spectra with the generalized version of Eq. 2 and find that both the coupling rate and the line width increase as the probing frequency increases. For the first harmonic ($\nu_0 = 7.65$ GHz) we find $\Omega = 85$ MHz and $\gamma = 19$ MHz, similar to the results of DPPH of the previous sections. For the second harmonic ($\nu \approx 2\nu_0$) we find two equivalent spin ensembles with $\Omega = 89$ MHz and $\gamma \approx 28$ MHz, as expected from the symmetry of the magnetic field profile. Finally, for the third harmonic ($\nu \approx 3\nu_0$) we have a further increase of the coupling rate and of the linewidth to $\Omega = 97$ MHz and $\gamma \approx 60$ MHz, respectively (here, for the central sub-ensemble). Electromagnetic simulations show a reduction of the effective number of spins in each sub-ensemble as the order of the harmonic increases. Therefore the increase in Ω is most likely due to the increase of the single spin coupling, due to the enhancement of b_1. Conversely, the increase of the linewidth is due to the enhanced inhomogeneities of the oscillating fields. Remarkably, for the

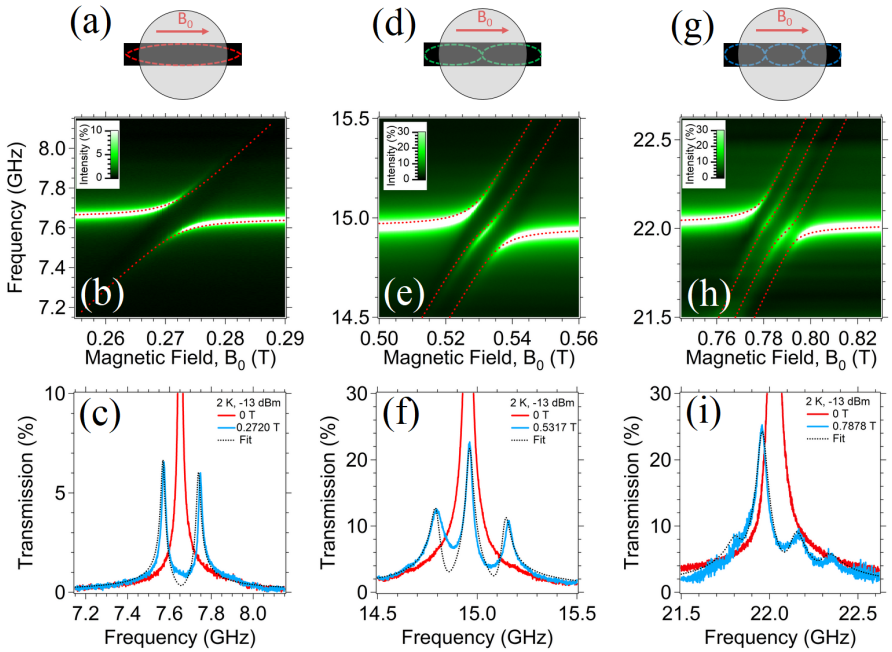

Figure 15. Transmission spectroscopic results for the coupling of an extended and concentrated DPPH pellet with the fundamental (a,b,c), the first (d,e,f) and the second (g,h,i) harmonic of a YBCO microstrip with $w = 700\mu$m, $L = 7$ mm at 2 K and $P_{in} = -13$ dBm. The number of mixed spin-photon mode increases with the order of the harmonic, as expected from the different magnetic field distributions of the $\lambda/2$ resonant modes (dashed lines in (a,d,g)). Dashed lines in (b,e,h) and (c,f,i) are fits based on Eq. 2 or on its generalization to the case of multiple spin ensembles [51].

second harmonic, the applied static magnetic field is $B_0 \approx 0.78$ T that is, to the best of our knowledge, one of the highest magnetic field at which high cooperativity has been observed with planar superconducting resonators.

6. Final Comparison

Fig. 16 summarizes the results presented so far and displays the key parameters characterizing the magnetic coupling between spin ensembles and microwave resonators. For each sample, the coupling rate Ω is plotted against the corresponding linewidth γ. Since in our experimental conditions $\gamma, \Omega > \kappa_0$, the weak and strong coupling regimes can be simply visualized below and above the $\Omega = \gamma$ dashed line respectively. The size of the symbols accounts for temperature, which spans from 50 K to 0.5 K (largest ones). Points taken from literature are added for comparison. In particular, we focus on the values reported for NV centers ([65] and blue rectangle) and Er^{3+} impurities in inorganic hosts ([67, 68] and green rectangle).
For diluted molecular spin systems, transition metal-based molecules, $Cu(mnt)_2$ and VOPc, exhibit higher Ω/γ ratios than the Lanthanide-based ones. This conclusion is probably not definitive since Rare Earths-based samples typically have higher Ω, resulting from their larger g-factors but, as a matter of facts, samples we have measured also exhibited larger γ due to the inhomogeneous broadening [31].
Overall, the effect of the dilution of the samples is visible and, although it helps in getting sharper lines, it results also in the reduction of the coupling rate. For certain

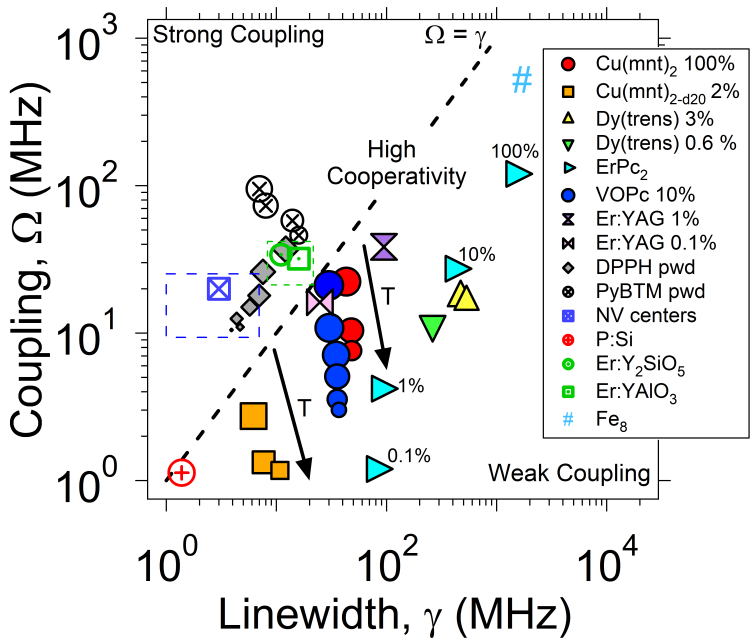

Figure 16. Plot of the collective coupling rates Ω as a function of the spin linewidth γ for the molecular spin samples discussed in this work (filled symbols). Best results obtained for the Er:YAG crystals are also added. The different sizes of the symbols denote the temperature, from 50 K (smaller one) down to 0.5 K (larger one). Dashed lines is the $\Omega = \gamma$ line, which denotes the crossover between the weak and the high cooperativity regime. Additional points for NV-centers [65], Er^{3+} ions [67, 68], P impurities in Si [80] and Fe_8 [81] obtained in similar spectroscopic experiments are shown for comparison. Dashed rectangles show the typical working ranges obtained for NV centers (blue) and Er^{3+} ions in inorganic crystals (green) at temperatures between 10 and 50 mK.

values of dilution the total benefit seems to be washed out.
The trend shown by Ω and γ as the temperature is decreased suggests that the crossover between the weak coupling and the high cooperativity regime can be reached by lowering the temperature. For 10 % VOPc:TiOPc solid dispersions, the high cooperativity regime is achieved at 0.5 K [82]. Worth to note is that the cooperativity value found at 0.5 K for this sample well compares to the one reported for NV-centers and Er^{3+}:YAG at lower temperatures (10-50 mK).
As concerns concentrated samples, the 100 % powders of DPPH and PyBTM organic radicals are clearly in the region of high cooperativity, in the whole temperature range between 2 to 50 K, and have C values up to 10^3 [27, 51]. Here, the exchange narrowing effect gives very sharp transitions that, together with the relatively high concentrations ($\approx 10^{20} : 10^{21}$ spin/cm^3, hence high Ω), result in the strong coupling regime [27, 41, 51].
Overall, this analysis reveals that the values of γ found in our experiments are mainly limited by the inhomogeneous broadening and not by the intrinsic relaxation rates of the molecular spins, suggesting that further margins for improvement are still possible.

7. Perspectives

Results presented in the previous sections are preliminary, albeit important, steps towards the integration of molecular spins in circuit-QED and they evidences some pros and cons in the use of molecular units in hybrid architectures. The research on this topic was driven by curiosity and amusement so far, yet there is an impelling request for developing new quantum technologies that can exploit the best characteristics and combination of different quantum systems. Although the field is at its infancy, several challenges can be clearly seen for the near future as briefly discussed in the following.
In the experiments described in the previous sections, we have used (large) ensembles of molecular spins to enhance the collective coupling with MW photons. Next challenge will be to coherently couple small ensembles and eventually one single (molecular) spin. This objective has been already achieved by using single electron spins in quantum dots [83, 84] but in this case the electric field component of the electromagnetic radiation was used. As we have already mentioned, the coupling of a single spin with the magnetic field component is much weaker and some strategies are needed to overcome this problem. One possibility is to enhance the g-factor and, to this purpose, the exploitation of spin-orbit effects and molecular engineering of the ligand field may lead to large g-factors and magnetic moments. If one manages to use one -or eventually few- spin(s) localized in space the magnetic component of the MW photons need to be concentrated in a small volume (see section 5.5) in order to enhance the coupling as suggested in [56]. In terms of a lumped element analogy, the inductive coupling between spin and MW circuit needs to be maximized, and this requires that the coupling inductance should be well detectable in the whole MW circuit. This strategy was recently used to couple an ensemble of 10^4 spins in ESR like experiments [85, 86]. The small number of spins requires the use of small number of photons in cavity with a consequent request of very low temperature and very long life time in cavity. In addition, detecting few MW photons requires the amplification of signal and extremely low level of noise [85–87]. These performances can be achieved nowadays with parametric amplifiers that make use of Josephson junctions [88]. These considerations lead us to conclude that the ambitious goal to address a single spin with MW photons does not seem to be impeded by fundamental barriers [89]

and some of the technical solutions are already available. One of the main advantages in using molecular spins with respect to other spin defects in inorganic matrices is represented by the possibility to precisely position and bind molecules to the active circuit element by using specific anchoring groups.
The use of superconducting circuits is assuming a central role in Quantum technologies since, besides the superconducting devices may encode qubits, planar resonators effectively work as quantum bus [90–92]. Here, the design of the circuit and the choice of superconducting materials can be crucial to obtain specific performances. While conventional superconductors are normally used to make low noise devices, the use of high-T_c superconductors can be interesting -even mandatory- for applications at finite temperature and in magnetic fields. Interestingly, YBCO films can be grown on silicon [93] and they can be patterned down to 50x50 nm^2 by essentially preserving excellent superconducting properties [94].
The possibility to coherently couple molecular spins with MW photons give us the chance to couple them with other quantum systems which, in turns, are coupled to the same superconducting bus. There is indeed a general consensus that next generation of quantum devices will probably use a hybrid architecture in which different quantum systems exchange information in a coherent way [95–98]. The energy levels and the states of molecular spins can be tailored almost at wish in order to work in weak magnetic field but their ESR transitions may also span over several MW bands. Our early steps along this line have been presented in the previous paragraphs, where we have shown how to spectroscopically distinct spin ensembles can be coupled by MW photons in the same cavity. Next challenge along this line could be to use similar MW photons to couple molecular spins with other quantum systems.
The high cooperative regime achieved by coupling (molecular) spins with MW photons is just a pre-requisite for their efficient manipulation in time domain. Next step along this line requires the use of pulse sequences that allow to store and retrieve qubits for a finite time [99, 100]. In particular, if properly optimized, MW pulse sequences can help to partially recover coherence that is inevitably lost during the encoding and transmission processes [54]. While the design of optimized pulse sequence is tailored to specific architectures, there is a general interest for developing protocols of universal use and in this context (molecular) spins can play an important role as test beds.

The challenges depicted here above are only few possible directions this research may take in the near future yet, we believe, they may give an idea of the potential richness of this emerging field.

Acknowledgement(s)

We would like to thank Dr. F. Troiani (CNR-Nano Modena), Prof. S. Carretta (Univ. Parma) and Prof. D. Gerace (Univ. Pavia), Prof. L. Sorace (Univ. Firenze) and Prof. R. Sessoli (Univ. Firenze), Prof. S. Hill (Florida State Univ.), Prof. T. Takui (Osaka City Univ.) for stimulating discussions.

Disclosure statement

Any options, finding, and conclusions or recommendations expressed in this material are those of the author(s) and do not necessarily reflect the views of the United States

Air Force.

Funding

This work was partially supported by the Italian Ministry of Education and Research (MIUR) though PRIN project 2015HYFSRT and based upon work partially supported by the Air Force Office of Scientific Research under award number FA2386-17-1-4040.

Nomenclature/Notation

(1) TLS = Two Level System
(2) ESR = Electron Spin Resonance
(3) CW = Continuous Wave
(4) PW = Pulsed Wave
(5) circuit-QED = circuit Quantum ElectroDynamics
(6) MW = Microwave
(7) VNA = Vector Network Analyzer
(8) Q = Quality factor, also referred as the unloaded one
(9) Q_L = Loaded quality factor
(10) L = Length of the resonant strip
(11) w = Width of the resonant strip
(12) s = Gap between the resonant strip and the lateral ground planes
(13) h = Planck's constant
(14) μ_B = Bohr's magneton
(15) γ_e = Gyromagnetic ration for the electron
(16) B_0 = Static magnetic Field
(17) B_1 = Magnetic component of the MW Field
(18) n = Mean photon number in the resonator
(19) $a, a^\dagger$ = Annihilation and creation operators for a single photon of the cavity
(20) S = Electronic spin (in unit of $\hbar$)
(21) I = Nuclear spin (in unit of $\hbar$)
(22) $\overrightarrow{S}$ = Spin operator
(23) $\overrightarrow{b_1}$ = Magnetic field generated by the resonator populated with a single photon
(24) $\sigma^{\pm}_{TLS}$ = Rising and lowering operator for the TLS
(25) ν_0 = Resonant frequency of the empty resonator (or cavity) in zero field
(26) ν_{TLS} = Zeeman transition energy for a TLS
(27) ν_S = Zeeman transition energy for a spin ensemble
(28) Ω_R = Rabi frequency for a TLS driven by B_0 and B_1
(29) Δ_c = Detuning between the probing frequency and the cavity frequency ν_0
(30) g = Landé g-factor
(31) κ = Total decay rate of the resonator
(32) κ_{ext} = External decay rate of the resonator
(33) κ_{int} = Internal decay rate of the resonator
(34) γ = Ensemble decay rate or linewidth (Half Width at Half Maximum linewidth, HWMH)
(35) γ_{hom} = Homogeneous contribution to the ensemble decay rate (HWMH)
(36) T_1 = Spin-phonon relaxation time
(37) T_2 = Spin-spin decoherence time

(38) Ω_{TLS} = Coupling rate between a TLS and a photon
(39) Ω = Magnetic collective coupling rate between a spin ensemble and photon(s)
(40) Ω_S = Single spin coupling rate
(41) N, N_{eff} = Effective number of spin involved in the collective coupling
(42) C = Cooperativity
(43) $p(T)$ = Spin polarization as function of temperature
(44) S_{21} = Scattering parameter from port 1 to port 2 (i.e. transmission from port 1 to port 2)
(45) S_{11} = Scattering parameter from port 1 to port 1 (i.e. reflection from port 1 back to port 1)
(46) IL = Insertion Loss

References

[1] P. Neumann, J. Beck, M. Steiner, F. Rempp, H. Fedder, P.R. Hemmer, J. Wrachtrup, and F. Jelezko, *Single-shot readout of a single nuclear spin*, Science 329 (2010), pp. 542–544, Available at http://science.sciencemag.org/content/329/5991/542.

[2] A. Laucht, J.T. Muhonen, F.A. Mohiyaddin, R. Kalra, J.P. Dehollain, S. Freer, F.E. Hudson, M. Veldhorst, R. Rahman, G. Klimeck, K.M. Itoh, D.N. Jamieson, J.C. McCallum, A.S. Dzurak, and A. Morello, *Electrically controlling single-spin qubits in a continuous microwave field*, Science Advances 1 (2015), Available at http://advances.sciencemag.org/content/1/3/e1500022.

[3] M. Veldhorst, C.H. Yang, J.C.C. Hwang, W. Huang, J.P. Dehollain, J.T. Muhonen, S. Simmons, A. Laucht, F.E. Hudson, K.M. Itoh, A. Morello, and A.S. Dzurak, *A two-qubit logic gate in silicon*, Nature 526 (2015), pp. 410–414, Available at http://dx.doi.org/10.1038/nature15263.

[4] E. Bernardi, R. Nelz, S. Sonusen, and E. Neu, *Nanoscale sensing using point defects in single-crystal diamond: Recent progress on nitrogen vacancy center-based sensors* 7 (2017).

[5] F. Shi, Q. Zhang, P. Wang, H. Sun, J. Wang, X. Rong, M. Chen, C. Ju, F. Reinhard, H. Chen, J. Wrachtrup, J. Wang, and J. Du, *Single-protein spin resonance spectroscopy under ambient conditions*, Science 347 (2015), pp. 1135–1138, Available at http://science.sciencemag.org/content/347/6226/1135.

[6] S. Probst, H. Rotzinger, S. Wünsch, P. Jung, M. Jerger, M. Siegel, A.V. Ustinov, and P.A. Bushev, *Anisotropic rare-earth spin ensemble strongly coupled to a superconducting resonator*, Phys. Rev. Lett. 110 (2013), p. 157001, Available at https://link.aps.org/doi/10.1103/PhysRevLett.110.157001.

[7] Y. Kubo, I. Diniz, A. Dewes, V. Jacques, A. Dréau, J.F. Roch, A. Auffeves, D. Vion, D. Esteve, and P. Bertet, *Storage and retrieval of a microwave field in a spin ensemble*, Phys. Rev. A 85 (2012), p. 012333, Available at https://link.aps.org/doi/10.1103/PhysRevA.85.012333.

[8] S. Nakazawa, S. Nishida, T. Ise, T. Yoshino, N. Mori, R.D. Rahimi, K. Sato, Y. Morita, K. Toyota, D. Shiomi, M. Kitagawa, H. Hara, P. Carl, P. HÃfer, and T. Takui, *A synthetic two-spin quantum bit: g-engineered exchange-coupled biradical designed for controlled-not gate operations*, Angewandte Chemie International Edition 51 (2012), pp. 9860–9864, Available at http://dx.doi.org/10.1002/anie.201204489.

[9] S. Suzuki, T. Furui, M. Kuratsu, M. Kozaki, D. Shiomi, K. Sato, T. Takui, and K. Okada, *Nitroxide-substituted nitronyl nitroxide and iminonitroxide*, Journal of the American Chemical Society 132 (2010), pp. 15908–15910, Available at http://dx.doi.org/10.1021/ja107769z, pMID: 20964296.

[10] C. Simão, M. Mas-Torrent, N. Crivillers, V. Lloveras, J.M. Artés, P. Gorostiza, J. Veciana, and C. Rovira, *A robust molecular platform for non-volatile memory devices*

with optical and magnetic responses, Nat Chem 3 (2011), pp. 359–364, Available at http://dx.doi.org/10.1038/nchem.1013.

[11] K. Bader, M. Winkler, and J. van Slageren, *Tuning of molecular qubits: very long coherence and spin-lattice relaxation times*, Chem. Commun. 52 (2016), pp. 3623–3626, Available at http://dx.doi.org/10.1039/C6CC00300A.

[12] M. Warner, S. Din, I.S. Tupitsyn, G.W. Morley, A.M. Stoneham, J.A. Gardener, Z. Wu, A.J. Fisher, S. Heutz, C.W.M. Kay, and G. Aeppli, *Potential for spin-based information processing in a thin-film molecular semiconductor*, Nature 503 (2013), pp. 504–508.

[13] M. Atzori, L. Tesi, E. Morra, M. Chiesa, L. Sorace, and R. Sessoli, *Room-temperature quantum coherence and rabi oscillations in vanadyl phthalocyanine: Toward multifunctional molecular spin qubits*, Journal of the American Chemical Society 138 (2016), pp. 2154–2157, Available at http://dx.doi.org/10.1021/jacs.5b13408, pMID: 26853512.

[14] M. Atzori, E. Morra, L. Tesi, A. Albino, M. Chiesa, L. Sorace, and R. Sessoli, *Quantum coherence times enhancement in vanadium(iv)-based potential molecular qubits: the key role of the vanadyl moiety*, Journal of the American Chemical Society 138 (2016), p. 1123411244, Available at http://dx.doi.org/10.1021/jacs.6b05574, pMID: 27517709.

[15] A. Ghirri, A. Candini, and M. Affronte, *Molecular spins in the context of quantum technologies*, Magnetochemistry 3 (2017), p. 12.

[16] A. Ghirri, J. van Tol, I. Vitorica-Yrezabal, G.A. Timco, and R.E.P. Winpenny, *Effects of the dzyaloshinskii-moriya interaction in cr3 triangular spin clusters detected by specific heat and multi-frequency electron spin resonance*, Dalton Trans. 44 (2015), pp. 14027–14033, Available at http://dx.doi.org/10.1039/C5DT01938A.

[17] F. Moro, D. Kaminski, F. Tuna, G.F.S. Whitehead, G.A. Timco, D. Collison, R.E.P. Winpenny, A. Ardavan, and E.J.L. McInnes, *Coherent electron spin manipulation in a dilute oriented ensemble of molecular nanomagnets: pulsed epr on doped single crystals*, Chem. Commun. 50 (2014), pp. 91–93, Available at http://dx.doi.org/10.1039/C3CC46326E.

[18] A.W. Eddins, C.C. Beedle, D.N. Hendrickson, and J.R. Friedman, *Collective coupling of a macroscopic number of single-molecule magnets with a microwave cavity mode*, Phys. Rev. Lett. 112 (2014), p. 120501, Available at https://link.aps.org/doi/10.1103/PhysRevLett.112.120501.

[19] S. Takahashi, J. van Tol, C.C. Beedle, D.N. Hendrickson, L.C. Brunel, and M.S. Sherwin, *Coherent manipulation and decoherence of $s = 10$ single-molecule magnets*, Phys. Rev. Lett. 102 (2009), p. 087603, Available at https://link.aps.org/doi/10.1103/PhysRevLett.102.087603.

[20] Y. Lan, S. Klyatskaya, M. Ruben, O. Fuhr, W. Wernsdorfer, A. Candini, V. Corradini, A. Lodi Rizzini, U. del Pennino, F. Troiani, L. Joly, D. Klar, H. Wende, and M. Affronte, *Magnetic interplay between two different lanthanides in a tris-phthalocyaninato complex: a viable synthetic route and detailed investigation in the bulk and on the surface*, J. Mater. Chem. C 3 (2015), pp. 9794–9801, Available at http://dx.doi.org/10.1039/C5TC02011E.

[21] K. Katoh, H. Isshiki, T. Komeda, and M. Yamashita, *Review*, Coordination Chemistry Reviews 255 (2011), pp. 2124–2148.

[22] G.A. Timco, S. Carretta, F. Troiani, F. Tuna, R.J. Pritchard, C.A. Muryn, E.J.L. McInnes, A. Ghirri, A. Candini, P. Santini, G. Amoretti, M. Affronte, and R.E.P. Winpenny, *Engineering the coupling between molecular spin qubits by coordination chemistry*, Nat Nano 4 (2009), pp. 173–178, Available at http://dx.doi.org/10.1038/nnano.2008.404.

[23] A. Candini, G. Lorusso, F. Troiani, A. Ghirri, S. Carretta, P. Santini, G. Amoretti, C. Muryn, F. Tuna, G. Timco, E.J.L. McInnes, R.E.P. Winpenny, W. Wernsdorfer, and M. Affronte, *Entanglement in supramolecular spin systems of two weakly coupled antiferromagnetic rings (purple-*$\mathbf{Cr_7}$Ni*)*, Phys. Rev. Lett. 104 (2010), p. 037203, Available at https://link.aps.org/doi/10.1103/PhysRevLett.104.037203.

[24] A. Bousseksou, G. Molnar, L. Salmon, and W. Nicolazzi, *Molecular spin crossover phenomenon: recent achievements and prospects*, Chem. Soc. Rev. 40 (2011), pp. 3313–3335, Available at http://dx.doi.org/10.1039/C1CS15042A.

[25] A. Ghirri, C. Bonizzoni, M. Righi, F. Fedele, G. Timco, R. Winpenny, and M.

Affronte, *Microstrip resonators and broadband lines for x-band epr spectroscopy of molecular nanomagnets*, Applied Magnetic Resonance (2015), pp. 1–8, Available at http://dx.doi.org/10.1007/s00723-015-0672-5.

[26] Z.L. Xiang, S. Ashhab, J.Q. You, and F. Nori, *Hybrid quantum circuits: Superconducting circuits interacting with other quantum systems*, Rev. Mod. Phys. 85,623 (2013), Available at http://link.aps.org/doi/10.1103/RevModPhys.85.623.

[27] A. Ghirri, C. Bonizzoni, D. Gerace, S. Sanna, A. Cassinese, and M. Affronte, *Yba2cu3o7 microwave resonators for strong collective coupling with spin ensembles*, Applied Physics Letters 106 (2015), 184101, Available at http://scitation.aip.org/content/aip/journal/apl/106/18/10.1063/1.4920930.

[28] R.N. Simons, *Coplanar Waveguide Circuits, Components, and Systems*, Wiley-Interscience, John Wiley & Son, Ltd, 2001.

[29] M.J. Lancaster, J.C. Li, A. Porch, and N.G. Chew, *High temperature superconductor lumped element resonator*, Electronics Letters 29 (1993), pp. 1728–1729.

[30] *Ceraco ceramic coating gmbh*, http://www.ceraco.de/hts-films/.

[31] C. Bonizzoni, A. Ghirri, K. Bader, J. van Slageren, M. Perfetti, L. Sorace, Y. Lan, O. Fuhr, M. Ruben, and M. Affronte, *Coupling molecular spin centers to microwave planar resonators: towards integration of molecular qubits in quantum circuits*, Dalton Trans. 45 (2016), pp. 16596–16603, Available at http://dx.doi.org/10.1039/C6DT01953F.

[32] C. Bonizzoni, A. Ghirri, M. Atzori, L. Sorace, R. Sessoli, and M. Affronte, *Coherent coupling between vanadyl phthalocyanine spin ensemble and microwave photons: towards integration of molecular spin qubits into quantum circuits*, Scientific Reports 7 (2017), p. 13096, Available at https://doi.org/10.1038/s41598-017-13271-w.

[33] J.M. Sage, V. Bolkhovsky, W.D. Oliver, B. Turek, and P.B. Welander, *Study of loss in superconducting coplanar waveguide resonators*, Journal of Applied Physics 109 (2011), 063915, Available at http://scitation.aip.org/content/aip/journal/jap/109/6/10.1063/1.3552890.

[34] K. Coakley, J. Splett, M. Janezic, and R. Kaiser, *Estimation of q-factors and resonant frequencies*, Microwave Theory and Techniques, IEEE Transactions on 51 (2003), pp. 862–868.

[35] C. Yang, Y. Xia, Y. Xue, F. Zhang, B. Tao, and J. Xiong, *The effects of grain boundaries on the current transport properties in ybco-coated conductors*, Nanoscale Research Letters 10 (2015), p. 416, Available at https://doi.org/10.1186/s11671-015-1124-8.

[36] A. Díaz, L. Mechin, P. Berghuis, and J.E. Evetts, *Evidence for vortex pinning by dislocations in yba2cu3o$_(7-\delta)$ low-angle grain boundaries*, Phys. Rev. Lett. 80 (1998), pp. 3855–3858, Available at https://link.aps.org/doi/10.1103/PhysRevLett.80.3855.

[37] M. Bauer, R. Semerad, and H. Kinder, *Ybco films on metal substrates with biaxially aligned mgo buffer layers*, IEEE Transactions on Applied Superconductivity 9 (1999), pp. 1502–1505.

[38] G. Boero, G. Gualco, R. Lisowski, J. Anders, D. Suter, and J. Brugger, *Room temperature strong coupling between a microwave oscillator and an ensemble of electron spins*, Journal of Magnetic Resonance 231 (2013), pp. 133 – 140, Available at http://www.sciencedirect.com/science/article/pii/S1090780713000979.

[39] I.I. Rabi, *Space quantization in a gyrating magnetic field*, Phys. Rev. 51 (1937), pp. 652–654, Available at http://link.aps.org/doi/10.1103/PhysRev.51.652.

[40] E. Jaynes and F. Cummings, *Comparison of quantum and semiclassical radiation theories with application to the beam maser*, Proceedings of the IEEE 51 (1963), pp. 89–109.

[41] I. Chiorescu, N. Groll, S. Bertaina, T. Mori, and S. Miyashita, *Magnetic strong coupling in a spin-photon system and transition to classical regime*, Phys. Rev. B 82 (2010), p. 024413, Available at http://link.aps.org/doi/10.1103/PhysRevB.82.024413.

[42] M. Tavis and F.W. Cummings, *Exact solution for an n-molecule¯radiation-field hamiltonian*, Phys. Rev. 170 (1968), pp. 379–384, Available at http://link.aps.org/doi/10.1103/PhysRev.170.379.

[43] M. Tavis and F.W. Cummings, *Approximate solutions for an n-molecule-*

radiation-field hamiltonian, Phys. Rev. 188 (1969), pp. 692–695, Available at http://link.aps.org/doi/10.1103/PhysRev.188.692.

[44] T. Holstein and H. Primakoff, *Field dependence of the intrinsic domain magnetization of a ferromagnet*, Phys. Rev. 58 (1940), pp. 1098–1113, Available at https://link.aps.org/doi/10.1103/PhysRev.58.1098.

[45] J.A. Weil and J.R. Bolton, *Electron Paramagnetic Resonance, elementar theory and applications*, John Wiley & Sons, 2007.

[46] A. Schweiger and G. Jeschke, *Principles of Paramagnetic Resonance*, Oxford University Press, 2001.

[47] A.M. Stoneham, *Shapes of inhomogeneously broadened resonance lines in solids*, Rev. Mod. Phys. 41 (1969), pp. 82–108, Available at https://link.aps.org/doi/10.1103/RevModPhys.41.82.

[48] D.F. Walls and G.J. Milburn, *Quantum Optics*, Springer, 2007.

[49] A.A. Clerk, M.H. Devoret, S.M. Girvin, F. Marquardt, and R.J. Schoelkopf, *Introduction to quantum noise, measurement, and amplification*, Rev. Mod. Phys. 82 (2010), pp. 1155–1208, Available at http://link.aps.org/doi/10.1103/RevModPhys.82.1155.

[50] X. Zhang, C.L. Zou, N. Zhu, F. Marquardt, L. Jiang, and H.X. Tang, *Magnon dark modes and gradient memory*, Nat Commun 6 (2015), p. 8914, Available at http://dx.doi.org/10.1038/ncomms9914.

[51] A. Ghirri, C. Bonizzoni, F. Troiani, N. Buccheri, L. Beverina, A. Cassinese, and M. Affronte, *Coherently coupling distinct spin ensembles through a high-T_c superconducting resonator*, Phys. Rev. A 93 (2016), p. 063855, Available at http://link.aps.org/doi/10.1103/PhysRevA.93.063855.

[52] I. Diniz, S. Portolan, R. Ferreira, J.M. Gérard, P. Bertet, and A. Auffèves, *Strongly coupling a cavity to inhomogeneous ensembles of emitters: Potential for long-lived solid-state quantum memories*, Phys. Rev. A 84 (2011), p. 063810, Available at http://link.aps.org/doi/10.1103/PhysRevA.84.063810.

[53] Z. Kurucz, J.H. Wesenberg, and K. Mølmer, *Spectroscopic properties of inhomogeneously broadened spin ensembles in a cavity*, Phys. Rev. A 83 (2011), p. 053852, Available at http://link.aps.org/doi/10.1103/PhysRevA.83.053852.

[54] S. Putz, D.O. Krimer, R. Amsüss, A. Volookaran, T. Nöbauer, J. Schmiedmayer, S. Rotter, and J. Majer, *Protecting a spin ensemble against decoherence in the strong coupling regime of cavity qed*, Nature Physics 10 (2014), pp. 720–724.

[55] R.H. Dicke, *Coherence in spontaneous radiation processes*, Phys. Rev. 93 (1954), pp. 99–110, Available at http://link.aps.org/doi/10.1103/PhysRev.93.99.

[56] M. Jenkins, T. Hümmer, M.J. Martínez-Pérez, J. García-Ripoll, D. Zueco, and F. Luis, *Coupling single-molecule magnets to quantum circuits*, New Journal of Physics 15 (2013), p. 095007, Available at http://stacks.iop.org/1367-2630/15/i=9/a=095007.

[57] A. Kushino, Y. Aoki, N.Y. Yamasaki, T. Namiki, Y. Ishisaki, T.D. Matsuda, T. Ohashi, K. Mitsuda, and T. Yazawa, *Erbium-doped yttrium aluminum garnet as a magnetic refrigerant for low temperature x-ray detectors*, Journal of Applied Physics 90 (2001), pp. 5812–5818, Available at http://dx.doi.org/10.1063/1.1415538.

[58] J.B. Gruber, J.R. Quagliano, M.F. Reid, F.S. Richardson, M.E. Hills, M.D. Seltzer, S.B. Stevens, C.A. Morrison, and T.H. Allik, *Energy levels and correlation crystal-field effects in* er^{3+}*-doped garnets*, Phys. Rev. B 48 (1993), pp. 15561–15573, Available at https://link.aps.org/doi/10.1103/PhysRevB.48.15561.

[59] M. Ball, G. Garton, M.J.M. Leask, D. Ryan, and W.P. Wolf, *Low-temperature magnetic properties of some rare-earth garnet compounds*, Journal of Applied Physics 32 (1961), pp. S267–S269, Available at http://dx.doi.org/10.1063/1.2000429.

[60] P.C.E. Stamp and A. Gaita-Arino, *Spin-based quantum computers made by chemistry: hows and whys*, J. Mater. Chem. 19 (2009), pp. 1718–1730, Available at http://dx.doi.org/10.1039/B811778K.

[61] M.J. Graham, J.M. Zadrozny, M. Shiddiq, J.S. Anderson, M.S. Fataftah, S. Hill, and D.E. Freedman, *Influence of electronic spin and spinorbit coupling on decoherence in mononu-*

clear transition metal complexes, Journal of the American Chemical Society 136 (2014), pp. 7623–7626, Available at http://dx.doi.org/10.1021/ja5037397, pMID: 24836983.

[62] K. Bader, D. Dengler, S. Lenz, B. Endeward, S.D. Jiang, P. Neugebauer, and J. Van Slageren, *Room temperature quantum coherence in a potential molecular qubit*, Nature Communications 5 5 (2014).

[63] S. Stoll and A. Schweiger, *Easyspin, a comprehensive software package for spectral simulation and analysis in {EPR}*, Journal of Magnetic Resonance 178 (2006), pp. 42 – 55, Available at http://www.sciencedirect.com/science/article/pii/S1090780705002892.

[64] J.M. Zadrozny, J. Niklas, O.G. Poluektov, and D.E. Freedman, *Multiple quantum coherences from hyperfine transitions in a vanadium(iv) complex*, Journal of the American Chemical Society 136 (2014), pp. 15841–15844, Available at http://dx.doi.org/10.1021/ja507846k, pMID: 25340518.

[65] D.I. Schuster, A.P. Sears, E. Ginossar, L. DiCarlo, L. Frunzio, J.J.L. Morton, H. Wu, G.A.D. Briggs, B.B. Buckley, D.D. Awschalom, and R.J. Schoelkopf, *High-cooperativity coupling of electron-spin ensembles to superconducting cavities*, Phys. Rev. Lett. 105 (2010), p. 140501, Available at http://link.aps.org/doi/10.1103/PhysRevLett.105.140501.

[66] Y. Kubo, F.R. Ong, P. Bertet, D. Vion, V. Jacques, D. Zheng, A. Dréau, J.F. Roch, A. Auffeves, F. Jelezko, J. Wrachtrup, M.F. Barthe, P. Bergonzo, and D. Esteve, *Strong coupling of a spin ensemble to a superconducting resonator*, Phys. Rev. Lett. 105 (2010), p. 140502, Available at http://link.aps.org/doi/10.1103/PhysRevLett.105.140502.

[67] S. Probst, H. Rotzinger, S. Wünsch, P. Jung, M. Jerger, M. Siegel, A.V. Ustinov, and P.A. Bushev, *Anisotropic rare-earth spin ensemble strongly coupled to a superconducting resonator*, Phys. Rev. Lett. 110 (2013), p. 157001, Available at http://link.aps.org/doi/10.1103/PhysRevLett.110.157001.

[68] A. Tkalčec, S. Probst, D. Rieger, H. Rotzinger, S. Wünsch, N. Kukharchyk, A.D. Wieck, M. Siegel, A.V. Ustinov, and P. Bushev, *Strong coupling of an* er^{3+}*-doped* $yalo_3$ *crystal to a superconducting resonator*, Phys. Rev. B 90 (2014), p. 075112, Available at http://link.aps.org/doi/10.1103/PhysRevB.90.075112.

[69] P.W. Anderson and P.R. Weiss, *Exchange narrowing in paramagnetic resonance*, Rev. Mod. Phys. 25 (1953), pp. 269–276, Available at http://link.aps.org/doi/10.1103/RevModPhys.25.269.

[70] E. Knapp, *Lineshapes of molecular aggregates, exchange narrowing and intersite correlation*, Chemical Physics 85 (1984), pp. 73 – 82, Available at http://www.sciencedirect.com/science/article/pii/S0301010484851745.

[71] G. Korteweg and L. van Reijen, *Fine-structure epr spectra of clusters of strongly exchange-coupled paramagnetic ions*, Journal of Magnetic Resonance (1969) 44 (1981), pp. 159 – 172, Available at http://www.sciencedirect.com/science/article/pii/0022236481901992.

[72] D. Bencini and D. Gatteschi, *Electron Paramagnetic Resonance of Exchange Coupled Systems*, 1990.

[73] P. Grobet, L.V. Gerven, A.V.D. Bosch, and J. Vansummeren, *Low temperature magnetic properties of solid {DPPH}*, Physica B+C 8688, Part 3 (1977), pp. 1132 – 1134, Available at http://www.sciencedirect.com/science/article/pii/0378436377908191.

[74] R. Verlinden, P. Grobet, and L.V. Gerven, *Low temperature magnetic properties of dpph.(c6d6)x? studied by {NMR} and {EPR}*, Chemical Physics Letters 27 (1974), pp. 535 – 539, Available at http://www.sciencedirect.com/science/article/pii/000926147480299X.

[75] G. Tosi, F.A. Mohiyaddin, H. Huebl, and A. Morello, *Circuit-quantum electrodynamics with direct magnetic coupling to single-atom spin qubits in isotopically enriched 28si*, AIP Advances 4 (2014), 087122, Available at http://scitation.aip.org/content/aip/journal/adva/4/8/10.1063/1.4893242.

[76] M. Mergenthaler, J. Liu, J.J. Le Roy, N. Ares, A.L. Thompson, L. Bogani, F. Luis, S.J. Blundell, T. Lancaster, A. Ardavan, G.A.D. Briggs, P.J. Leek, and

E.A. Laird, *Strong coupling of microwave photons to antiferromagnetic fluctuations in an organic magnet*, Phys. Rev. Lett. 119 (2017), p. 147701, Available at https://link.aps.org/doi/10.1103/PhysRevLett.119.147701.

[77] P.J. Leek, M. Baur, J.M. Fink, R. Bianchetti, L. Steffen, S. Filipp, and A. Wallraff, *Cavity quantum electrodynamics with separate photon storage and qubit readout modes*, Phys. Rev. Lett. 104 (2010), p. 100504, Available at https://link.aps.org/doi/10.1103/PhysRevLett.104.100504.

[78] A.T. Asfaw, A.J. Sigillito, A.M. Tyryshkin, T. Schenkel, and S.A. Lyon, *Multi-frequency spin manipulation using rapidly tunable superconducting coplanar waveguide microresonators*, Applied Physics Letters 111 (2017), p. 032601, Available at http://dx.doi.org/10.1063/1.4993930.

[79] S.J. Bosman, M.F. Gely, V. Singh, A. Bruno, D. Bothner, and G.A. Steele, *Multi-mode ultra-strong coupling in circuit quantum electrodynamics*, npj Quantum Information 3 (2017), pp. 46–, Available at https://doi.org/10.1038/s41534-017-0046-y.

[80] C.W. Zollitsch, K. Mueller, D.P. Franke, S.T.B. Goennenwein, M.S. Brandt, R. Gross, and H. Huebl, *High cooperativity coupling between a phosphorus donor spin ensemble and a superconducting microwave resonator*, Applied Physics Letters 107 (2015), 142105, Available at http://scitation.aip.org/content/aip/journal/apl/107/14/10.1063/1.4932658.

[81] A.W. Eddins, C.C. Beedle, D.N. Hendrickson, and J.R. Friedman, *Collective coupling of a macroscopic number of single-molecule magnets with a microwave cavity mode*, Phys. Rev. Lett. 112 (2014), p. 120501, Available at http://link.aps.org/doi/10.1103/PhysRevLett.112.120501.

[82] C. Bonizzoni, A. Ghirri, M. Atzori, L. Sorace, R. Sessoli, and M. Affronte, *Coherent coupling between vanadyl phthalocyanine spin ensemble and microwave photons: towards integration of molecular spin qubits into quantum circuits*, Scientific Reports 7 (2017), p. 13096.

[83] X. Mi, J.V. Cady, D.M. Zajac, P.W. Deelman, and J.R. Petta, *Strong coupling of a single electron in silicon to a microwave photon*, Science 355 (2017), pp. 156–158, Available at http://science.sciencemag.org/content/355/6321/156.

[84] J.J. Viennot, M.C. Dartiailh, A. Cottet, and T. Kontos, *Coherent coupling of a single spin to microwave cavity photons*, Science 349 (2015), pp. 408–411, Available at http://www.sciencemag.org/content/349/6246/408.abstract.

[85] C. Eichler, A.J. Sigillito, S.A. Lyon, and J.R. Petta, *Electron spin resonance at the level of* 10^4 *spins using low impedance superconducting resonators*, Phys. Rev. Lett. 118 (2017), p. 037701, Available at https://link.aps.org/doi/10.1103/PhysRevLett.118.037701.

[86] BienfaitA., P. J., KuboY., SternM., ZhouX., L. C., W. D., SchenkelT., T.L. W., VionD., EsteveD., JulsgaardB., MølmerK., M.J. L., and BertetP., *Reaching the quantum limit of sensitivity in electron spin resonance*, Nat Nano 11 (2016), pp. 253–257, Available at http://dx.doi.org/10.1038/nnano.2015.282.

[87] S. Probst, A. Bienfait, P. Campagne-Ibarcq, J.J. Pla, B. Albanese, T. Da Silva Barbosa J. F.; Schenkel, D. Vion, D. Esteve, K. Mølmer, J.J.L. Morton, R. Heeres, and P. Bertet, *Inductive-detection electron-spin resonance spectroscopy with* **65** *spins/*$\sqrt{hz}$ *sensitivity*, ArXiv e-prints (2017), p. 1708.09287.

[88] A. Roy and M. Devoret, *Introduction to parametric amplification of quantum signals with josephson circuits*, Comptes Rendus Physique (2016), pp. 740–755.

[89] P. Haikka, Y. Kubo, A. Bienfait, P. Bertet, and K. Mølmer, *Proposal for detecting a single electron spin in a microwave resonator*, Phys. Rev. A 95 (2017), p. 022306, Available at https://link.aps.org/doi/10.1103/PhysRevA.95.022306.

[90] J. Majer, J.M. Chow, J.M. Gambetta, J. Koch, B.R. Johnson, J.A. Schreier, L. Frunzio, D.I. Schuster, A.A. Houck, A. Wallraff, A. Blais, M.H. Devoret, S.M. Girvin, and R.J. Schoelkopf, *Coupling superconducting qubits via a cavity bus*, Nature 449 (2007), pp. 443–447, Available at http://dx.doi.org/10.1038/nature06184.

[91] M. Sillanpää, J. Park, and R. Simmonds, *Coherent quantum state storage and transfer*

between two phase qubits via a resonant cavity, NATURE 449 (2007), pp. 438–442.

[92] G.K. Brennen, D. Song, and C.J. Williams, *Quantum-computer architecture using nonlocal interactions*, Phys. Rev. A 67 (2003), p. 050302, Available at https://link.aps.org/doi/10.1103/PhysRevA.67.050302.

[93] A. Mogro-Campero, *A review of high-temperature superconducting films on silicon*, Superconductor Science and Technology 3 (1990), p. 155, Available at http://stacks.iop.org/0953-2048/3/i=4/a=001.

[94] R. Arpaia, S. Nawaz, F. Lombardi, and T. Bauch, *Improved nanopatterning for ybco nanowires approaching the depairing current* 23 (2013).

[95] P. Rabl, D. DeMille, J.M. Doyle, M.D. Lukin, R.J. Schoelkopf, and P. Zoller, *Hybrid quantum processors: Molecular ensembles as quantum memory for solid state circuits*, Phys. Rev. Lett. 97 (2006), p. 033003, Available at https://link.aps.org/doi/10.1103/PhysRevLett.97.033003.

[96] R.J. Schoelkopf and S.M. Girvin, *Wiring up quantum systems*, Nature 451 (2008), pp. 664–669, Available at http://dx.doi.org/10.1038/451664a.

[97] G. Kurizki, P. Bertet, Y. Kubo, K. Mølmer, D. Petrosyan, P. Rabl, and J. Schmiedmayer, *Quantum technologies with hybrid systems*, Proceedings of the National Academy of Sciences 112 (2015), pp. 3866–3873, Available at http://www.pnas.org/content/112/13/3866.abstract.

[98] M.H. Devoret and R.J. Schoelkopf, *Superconducting circuits for quantum information: An outlook*, Science 339 (2013), pp. 1169–1174, Available at http://science.sciencemag.org/content/339/6124/1169.

[99] H. Wu, R.E. George, J.H. Wesenberg, K. Mølmer, D.I. Schuster, R.J. Schoelkopf, K.M. Itoh, A. Ardavan, J.J.L. Morton, and G.A.D. Briggs, *Storage of multiple coherent microwave excitations in an electron spin ensemble*, Phys. Rev. Lett. 105 (2010), p. 140503, Available at https://link.aps.org/doi/10.1103/PhysRevLett.105.140503.

[100] C. Grezes, B. Julsgaard, Y. Kubo, M. Stern, T. Umeda, J. Isoya, H. Sumiya, H. Abe, S. Onoda, T. Ohshima, V. Jacques, J. Esteve, D. Vion, D. Esteve, K. Mølmer, and P. Bertet, *Multimode storage and retrieval of microwave fields in a spin ensemble*, Phys. Rev. X 4 (2014), p. 021049, Available at https://link.aps.org/doi/10.1103/PhysRevX.4.021049.